THE EFFECT OF STRESS AND TEMPERATURE ON THE VELOCITY OF DISLOCATIONS IN PURE IRON MONOCRYSTALS

Thesis by

Arthur P. L. Turner

In Partial Fulfillment of the Requirements

For the Degree of

Doctor of Philosophy

California Institute of Technology

Pasadena, California

1969

(Submitted September 24, 1968)

ACKNOWLEDGMENTS

The author wishes to thank Professor Thad Vreeland Jr. for his aid and guidance throughout the course of this research. Appreciation is also extended to Professor D. S. Wood, Dr. D. P. Pope, Dr. J. A. Gorman, and Dr. R. C. Blish, whose helpful advice greatly facilitated various aspects of this work.

The author would also like to thank the Fannie and John Hertz Foundation for fellowship support during the period of this research and the Atomic Energy Commission for support of the experimental work.

Special thanks are extended to my wife, Marianne, for her encouragement and patience.

ABSTRACT

The velocity of dislocations in pure iron monocrystals as a function of applied stress was measured by observing the change in length of dislocation slip bands after the application of a constant stress amplitude load pulse. Measurements covered a range of stresses from 10 to 500 Mdynes/cm^2 and temperatures of 393, 295, 198, and 77°K.

The dislocation velocity at constant stress was found to be a sensitive function of temperature. However, the nature of the variation of the velocity with temperature was found to be inconsistent with theoretical formulations of thermally assisted dislocation motion. The nature of the disagreement between the experimental results and the thermal activation models is similar to that previously observed in niobium and Fe-3°/oSi . The decrease in dislocation velocity with decreasing temperature was also found to be too large to be attributed to hardening from the small amounts of impurities in the crystals.

The behavior of the dislocations as determined by this study was found to be consistent with predictions made from measurements of the macroscopic yield stress. However, the results of this study differ markedly from the behavior predicted from measurements of the strain rate sensitivity of the flow stress.

TABLE OF CONTENTS

LIST OF FIGURES

LIST OF TABLES

I. INTRODUCTION

A great deal of work has been done which attempts to relate the temperature dependence of the yield stress in iron and steel to the behavior of individual dislocations. The first mechanism proposed by Cottrell and Bilby (1)* and later refined by Fisher (2) was the thermally assisted release of dislocations from atmospheres of impurity atoms. However, other investigators (3 - 5) showed that pre-yield micro-strain, lower yield stress, and flow stress at large strains exhibit the same temperature dependence as the upper yield stress. These observations seemed to indicate that the temperature dependence of the flow stress in iron is more closely related to the properties of free moving dislocations than to the freeing of pinned dislocations. Therefore, it was concluded that the motion of free dislocations in iron and other BCC materials must be controlled by a thermally activated process. This conclusion was given additional support when Stein and Low (6) showed by direct measurement of dislocation velocities in Fe - 3°/o Si alloy that the relationships between dislocation velocity and resolved shear stress are strongly temperature dependent.

Three thermal activation controlled processes have been proposed as the mechanism which limits dislocation motion in BCC materials (7):

1. Non-conservative motion of jogs on screw dislocations (8);
2. Overcoming the Peierls-Nabarro (Peierls) energy bar-

---

* Numbers appearing in parentheses indicate references listed at the end of the thesis.

rier (9 - 11);

3. Overcoming the energy barriers of a random dispersion of impurities (12 - 14).

Each of these processes can be assisted by the thermal fluctuations of the crystal. Therefore, each gives rise to a dislocation velocity with the following functional form:

$$v = v_o(T, \tau) \exp\left(\frac{-U(T, \tau)}{kT}\right), \qquad [1]$$

where v is the dislocation velocity, k is the Boltzmann constant, T is the absolute temperature, and τ is the resolved shear stress tending to move the dislocation. The activation energy (U) and the limiting velocity (v_o) are quantities which depend on the mechanism. U and v_o are generally functions of temperature and stress.

Each of the above mechanisms is supported by some experimental evidence. However, the first mechanism would require a very high density of jogs and is generally considered to be the least likely of the three. Each of the latter two mechanisms has received considerable attention in recent years in terms of both theoretical and experimental treatments (10, 11, 13 - 22). However, the predicted behavior of dislocations from the two mechanisms is so similar that it has so far been impossible to unambiguously determine the dominant mechanism.

The Peierls energy barrier, which was first proposed by Orowan (23) and calculated by Peierls (24) and later refined by Nabarro (25) arises from the fact that the energy of a dislocation varies with its position in the unit cell of the lattice. Because of this variation,

the dislocation moving through the lattice experiences a periodic force with period b* where b is the magnitude of the slip vector and the spacing of equivalent sites for the dislocation. Since the Peierls energy depends on the imperfectly known interatomic forces in the crystal, calculations of its magnitude are subject to a considerable error. Therefore, most models which treat the Peierls energy attempt only to predict the nature of the activation process, leaving to experiment the determination of the magnitudes of the quantities involved.

The theory of the motion of a dislocation through a material with a large Peierls energy was first introduced by Seeger (16) and has since been treated by many others (17 - 20). The basic premise of all treatments is that in a material with sufficiently high Peierls energy, dislocations lie predominantly in the low energy positions of the lattice. Motion of the dislocation takes place when thermal fluctuations of the crystal aided by the applied stress activate a segment of the dislocation over the energy barrier into the next "Peierls valley." If a critical length is activated, motion of the rest of the dislocation occurs by growth of the length of the activated segment. Thus, for the Peierls mechanism, the activation energy is the energy required to move a critical length of dislocation across the barrier. v_o is the product of the attempt frequency and the distance moved per activation. For this model, the stress and temperature dependence of v_o

---

* Actually, the distance between low energy sites is not necessarily equal to b for screw dislocations. However, for simplicity, it is assumed equivalent for both edge and screw dislocations in this discussion.

can generally be ignored, but the activation energy has a complex stress dependence which depends on the shape of the barrier and the critical segment configuration.

The mechanism of solution hardening in BCC materials was first mentioned by Nabarro (26) and extended by Fleischer (13) and Kumar (15). The hardening arises from the fact that interstitial impurities in the BCC lattice produce large asymmetric distortions. Therefore, the solute atoms interact strongly with the stress field of a dislocation. In this case, a dispersion of solute atoms acts as a series of obstacles which, at low stresses, the dislocation can move through only with the aid of thermal activation. Like the Peierls energy, the interaction energy of the dislocation with the impurity atoms is difficult to calculate exactly, especially at very close distances of approach where linear elasticity theory cannot be assumed to hold. In addition, the interstitial atoms form a random array of obstacles, and so, unlike the case of regular Peierls barriers, the behavior of a dislocation moving through an array of impurity obstacles depends on the statistics of the distribution (27, 28). This once again gives rise to a model where the activation energy is dependent on the applied stress, but where the functional form of the dependence is not well understood.

A great deal of work has been done which purports to measure the dislocation velocity in iron (6, 10, 11, 21, 29 - 32). However, the vast majority of the work involves the inference of the dislocation velocity from some other measured property. This always requires assumptions about non-measurable quantities. The methods which

have been used to infer dislocation velocity include measurement of:

1. yield stress
2. microstrain
3. creep rates
4. internal friction
5. stress relaxation at constant total strain
6. stress changes for an instantaneous change in strain rate.

All methods involve an assumption of the density of moving dislocations in order to infer the dislocation velocity from measured parameters. Furthermore, the association of a free dislocation velocity with quantities measured by the above methods depends on the assumption that the same mechanism is rate controlling throughout the early part of the stress strain curve up to a few percent strain. This last assumption is highly questionable in view of evidence (33) that the dislocation velocity parameters inferred from measurements of types 1 and 2 depend strongly on the sensitivity of the measurement of plastic strain. Methods 5 and 6 have also been shown to depend on the amount of workhardening which has taken place.

Although the form of equation [1] is quite general, various investigators have found that experimental results often do not fit the theoretical expression. They have therefore introduced the idea that athermal processes occur similtaneously with the thermal activation of the dislocations. The effect of these processes is to produce a drag force on the dislocations. This drag force is included in the theoretical expressions by replacing the applied stress by the quantity $\tau^* = \tau_a - \tau_i$ where τ^* is the effective stress, τ_a the applied

stress, and τ_i is the equivalent of the athermal drag. Although τ_i is taken to be a constant, theoretical calculations (34) show that an internal stress field which varies with position in the body and has a zero average value will also reduce the average velocity of the dislocations. It is quite probable that such athermal processes do indeed occur within crystals during plastic deformation. However, since in practice the magnitude of τ_i is not known from independent measurements, τ_i is essentially another adjustable parameter which can be varied to obtain a best fit between theoretical expressions and experimental results. The practical effect of the introduction of τ_i is the elimination of any possibility of separating the mechanisms of Peierls and impurity hardening by comparison with the results of the already ambiguous experiments described above.

The unfortunate result of the ambiguity of the experimental evidence and the flexibility of the theories is that too often authors start by assuming the validity of their favorite theory, adjust the parameters of the theory to fit the experimental results, and finally by somewhat circular reasoning conclude by claiming the good fit of experiment to theory as proof of the validity of the theory (35). The issue is further confused when authors can include or neglect the possibility of a temperature dependence for U and v_o with little theoretical justification for either position (36, 37).

The present work was conceived as a step in making a critical test to see if the dominant mechanism for limiting dislocation velocity could be determined. The single factor which should be able to distinguish between the two popular theories is the effect of interstitial

impurity content on dislocation velocity. However, an experiment designed to show the presence or absence of an impurity concentration effect must be free from as many sources of controversy as possible if it is to be convincing. For example, assume that the iron test material contains both a substitutional and an interstitial impurity which can combine to form a precipitate. If the dislocation velocity decreases as the interstitial impurity content is increased, the advocates of the Peierls model can attribute the change in velocity to an increase in the internal stress from more numerous and larger precipitates. Conversely, if no effect on the dislocation velocity is observed, the advocates of impurity hardening can claim that the additional interstitial impurity was entirely locked up in precipitates and had very little effect on the concentration of impurities in solution. This consideration made it clear that the critical experiments should be done on the most pure material which was practical.

Since all determinations of dislocation velocity from measurements of macroscopic parameters, such as yield stress or the dependence of the flow stress on the strain rate, are so subject to differences in interpretation, it was also clear that any experiment which would convincingly show the effect of carbon concentration on dislocation velocity in iron would have to be based on direct observation of the dislocation displacements in a pulse loading type of test. Because no directly measured dislocation velocity data were available for pure iron, the measurement of the dislocation mobility in a high-purity single crystal of iron was the logical first step in an eventual study of the impurity effect.

In addition to laying a good foundation for later direct measurement of the impurity effect, it was hoped that the present study could answer additional questions immediately. First, it was hoped that the measurements could confirm or refute the assumption that a single thermally activated mechanism is rate controlling at all temperatures in pure iron. Secondly, if a single process was found to be controlling, are the values of the parameters of the mechanism consistent with those inferred from less direct measurements?

II. EXPERIMENTAL TECHNIQUES

Test Specimens

The original material for the test specimens was a single crystal which was grown and purified by D. F. Stein of the General Electric Research Laboratory. The crystal was grown by the strain anneal technique (38) from high purity iron sheet. After growth, the crystal was purified by heating it in a pure hydrogen atmosphere. The hydrogen was continuously purified by circulating it over a hot ZrH_2 getter (39). Other investigators (39, 40) have shown that this technique will reduce the concentration of carbon to less than 0.005 ppm and the levels of O and N to a few ppm by weight. The crystal as received from General Electric was approximately 10 cm long, 3.5 cm wide, and 0.125 cm thick. The normal to the sheet was oriented approximately 15° from a $\langle 110 \rangle$ direction.

Disc-shaped test specimens were prepared from the parent crystal by a combination of electric spark discharge and electrochemical machining techniques. Discs 0.63 cm diameter were first trepanned from the sheet by spark discharge machining. In order to ensure that the specimens would be free from damage when completed, the remainder of the machining was done by a special electrochemical technique.

The electrolapping technique, which is described in detail in Appendix A, electroplates iron from the specimen onto a spinning stainless steel plate through a thin film of 1M $FeCl_2$ solution. The advantages of this method are that it allows precise control of the machining and permits preparation of flat surfaces with very little

rounding of corners, even on small specimens.

Using the electrolapping machine as a lathe, the specimens were reduced to 0.475 cm diameter in order to remove the damage from the spark discharge machining. Then the electrochemical method was used to finish the faces of the disc. In this operation, the initial 15° misorientation of the discs was partially corrected as explained below.

The ideal orientation of the test specimen would have been with the face of the disc parallel to the (110) plane because this was expected to be the slip plane. However, because of the large misorientation of the parent crystal, it was not possible to fully correct the misorientation. Instead, a partial correction was made which resulted in the surface being 7° - 8° from (110), with the $[1\bar{1}1]$ direction lying in the specimen surface. The orientation and dimensions of the completed specimens are shown in Figure 1.

After they were cut to the proper shape, the specimens were electropolished in a solution composed of:

20 gm	Cr_2O_3
106 ml	Glacial Acetic Acid
6 ml	H_2O

The solution was maintained at a temperature between 16 - 18°C and was stirred during the polishing. The specimens were polished for 10 - 20 min at 17 volts potential between the specimen and the stainless steel cathode. Finally, the specimens were annealed for 48 - 96 hr in an atmosphere of hydrogen purified by diffusion through paladium in a commercially available diffusion unit. The temperature was

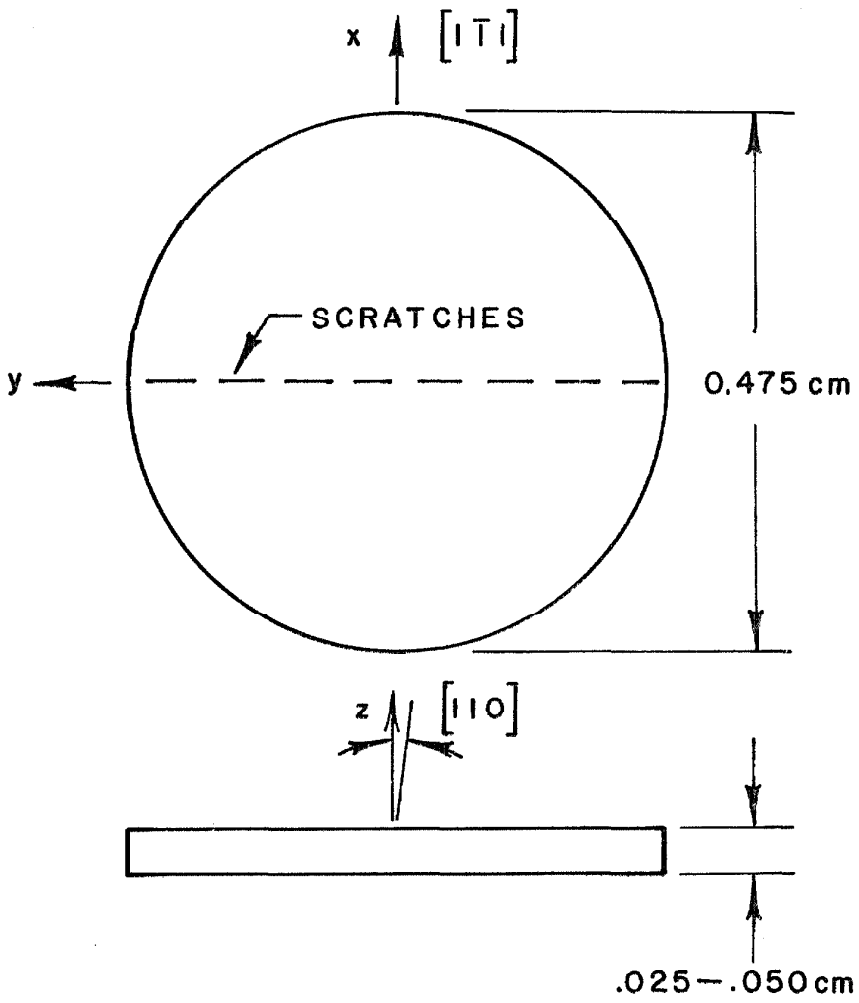

Figure 1. Dimensions and Orientation of Test Specimens.

oscillated between 880°C and 700°C in a 2.5 hr cycle. Specimens which were used for more than one test were also given the polishing and annealing treatment between tests.

Loading Machine

In order to carry out these tests in torsion, the rapid load testing machine developed by Russel and Wood (41) was modified to apply a pure torque. The torsion testing machine is shown schematically in Figure 2 and is shown pictured in Figure 3. Two shim steel straps 1.27 × 0.0025 cm carry the load from the piston of the rapid load machine to the torsion specimen. One of the straps passes around a fixed pulley to change the direction of the force. The straps are then attached around a tube which has a hexagonal socket on the inside. The specimen to be tested is bonded between two rods with hexagonal ends. One hexagonal end fits into the socket of the tube. The other hexagonal end fits into a similar socket fixed to the bottom of the testing machine. Since the two straps pull on the tube in opposite directions with equal force, a pure moment is applied to the torque tube. This moment is transmitted as torsion through the specimen to the fixed socket. Figure 4 shows the specimen bonded between the hexagonal torque application rods.

Figure 5 shows a typical load-time record for a 0.1 sec pulse. Trace 1 is the tensile load measured by a strain gauge dynamometer attached to the load machine piston. Trace 2 is the moment measured by a torsion strain gauge dynamometer used in place of the specimen to generate this record. The characteristic rise time of the

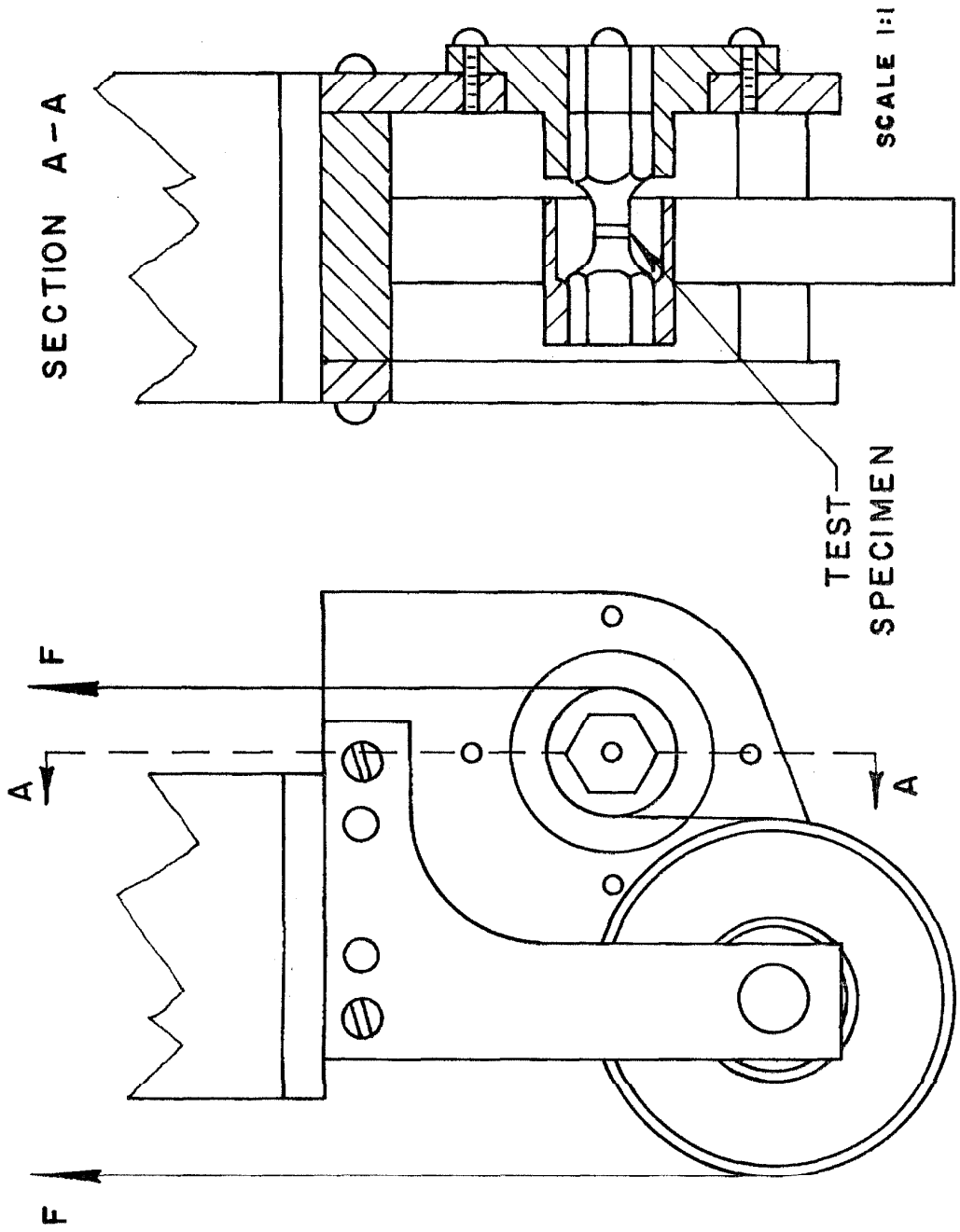

Figure 2. Drawing of Torsion Adapter for Rapid Load Testing Machine. Arrows Marked F Indicate Direction of Force Applied to Load Straps by Load Machine Piston.

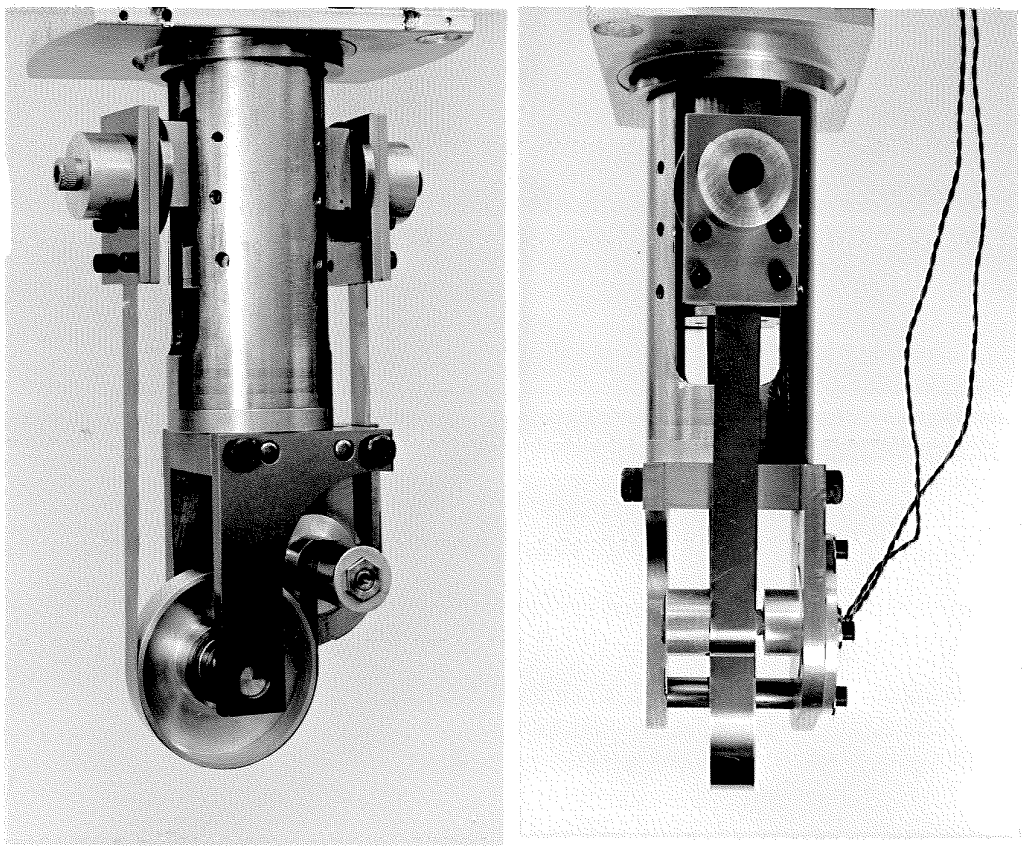

(a) (b)

Figure 3. Photograph of Torsion Adapter for Rapid Load Testing Machine. (Wires in View (b) are for Torsion Dynamometer Used Here in Place of Specimen.)

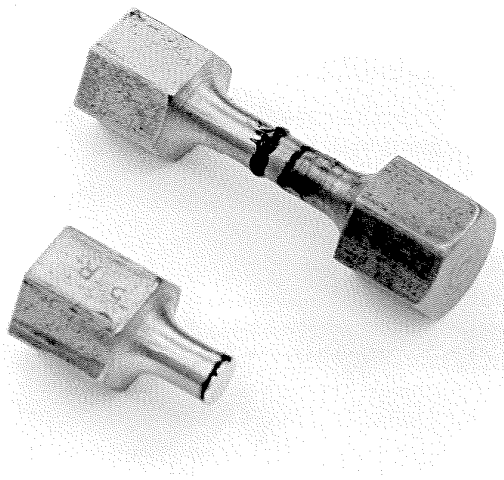

Figure 4. Test Specimen Mounted on Torsion Transmission Rod and Complete Specimen Assembly Ready to Test.

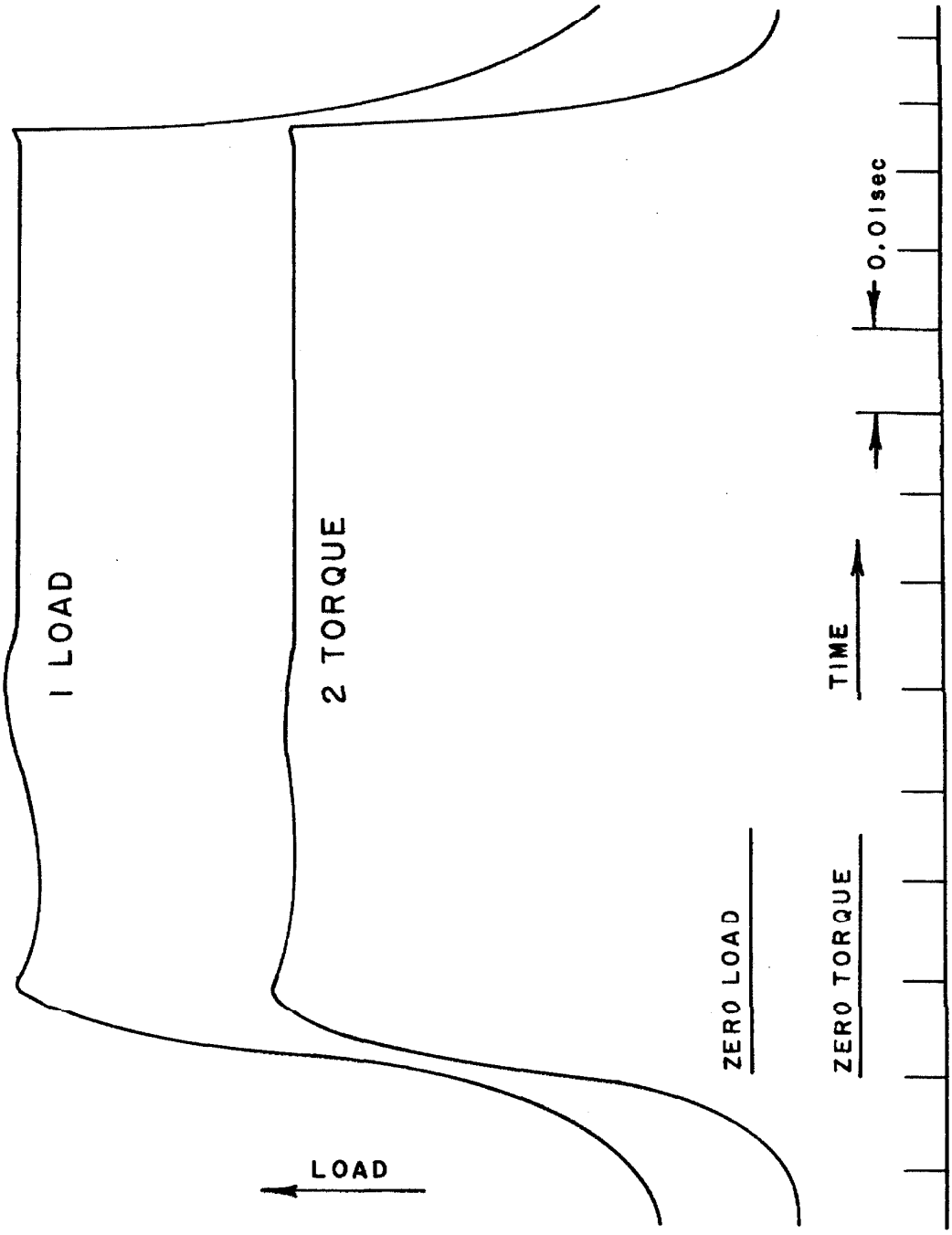

Figure 5. Typical Load vs. Time Record for Rapid Load Testing Machine Torsion Adapter. Trace 1 - Tensile Load; Trace 2 - Torque.

load with the torsion equipment is 0.030 sec. The length of the pulse is variable in increments of 0.017 sec from minimum time of 0.017 sec. Since the rise time is slower than this, a 0.017 sec pulse would be a triangular spike. Therefore, the minimum practical pulse was 0.068 sec, for which half of the time is rise time.

Stress State

A torsion type of test was chosen for these experiments when it was believed that the test specimens could be oriented with the slip plane parallel to the free surface. As stated above, the misorientation of the parent crystal was too great to allow preparation of specimens with the ideal orientation. Therefore, it was not possible to observe the motion of long lengths of dislocations as in tests on zinc by Pope, et al. (42) and on aluminum by Gorman, et al. (43). However, even for the misoriented crystals, the torsion stress state has the advantages of a stress gradient in the specimen and small specimen size.

If constraints of the displacements of the anisotropic crystal are ignored, the stress distribution for the anisotropic torsion problem is identical to that of an isotropic circular rod in torsion. However, the displacements of the anisotropic specimen included a warping function as for an elliptical isotropic rod in torsion. In the test situation, the specimen is bonded between two isotropic rods which constrain the displacements in the specimen. Therefore, the stress state in the test specimen is not the isotropic stress state. However, as discussed in more detail in Appendix B, the approximation of using

the isotropic torsion stress distribution does not cause a very large error in terms of the resolved shear stress on the dislocations. Furthermore, all data were measured at geometrically similar positions in the specimen with regard to the angle θ. This means that the error introduced by assuming the isotropic stress state might change the absolute magnitudes of the stress-velocity relationships, but should have a smaller effect on the functional form of the relationship.

Using the simplification that the stresses are the same as for a circular isotropic rod in torsion, the stress in terms of the total moment (M) is:

$$\tau_{\theta z} = \frac{2Mr}{\pi r_o^4} \quad , \qquad [2]$$

where r_o is the radius of the specimen. In a cartesian coordinate system where the Burgers vector is parallel to the x-axis and the slip plane is perpendicular to the z-axis, the resolved shear stress (τ_r) on a dislocation is:

$$\tau_r = \frac{2My}{\pi r_o^4} \quad . \qquad [3]$$

Figure 1 shows the relationship of the specimen geometry to the stress geometry. Note that edge dislocations produced by a radial scratch perpendicular to the Burgers vector move such that they experience a constant resolved shear stress.

Observation of the Dislocations

The B-B x-ray topographic method was used to observe the dislocation configuration. The theory and techniques for observation

of dislocations by the B-B x-ray method are described in detail elsewhere (44 - 46) so the method will only be briefly described here. The arrangement for the B-B method is shown schematically in Figure 6. A divergent beam of x-rays from source (A) strikes the observation surface of the specimen (B). The specimen is oriented so that the characteristic wavelength of the radiation satisfies the Bragg condition for a set of planes (dashed lines) in the specimen crystal. The diffracted beam then forms an image of the specimen on a film (C) placed very close to the specimen and nearly parallel to the incident x-ray beam. Slits (D) prevent the incident beam from exposing the film.

Dislocations are revealed by this technique because the disruption of the lattice periodicity near a dislocation causes an abnormally strong reflection from the dislocation sites. In the first order approximation, the contrast at a dislocation disappears for reflections from planes which contain the Burgers vector of the dislocation. This leads to the condition that dislocations will be visible in images where:

$$\bar{b} \cdot \bar{n} \neq 0 \ . \qquad [4]$$

$\bar{b}$ is the Burgers vector of the dislocation, and $\bar{n}$ is the normal of the reflecting planes.

Chromium K_α radiation was selected for this study, and all pictures were taken with a 0.025 mm thick vanadium foil between the specimen and the film to filter out the iron K_α fluorescence from the specimen. Figure 7 shows a stereographic projection of the crystal centered on the observation surface of the specimen. The circles on

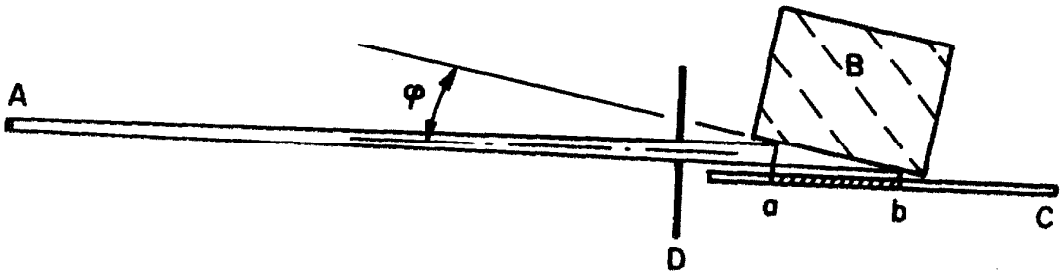

Figure 6. Schematic Diagram of B-B Method. A - X-ray Source; B - Specimen Crystal; C - Film; D - Slits.

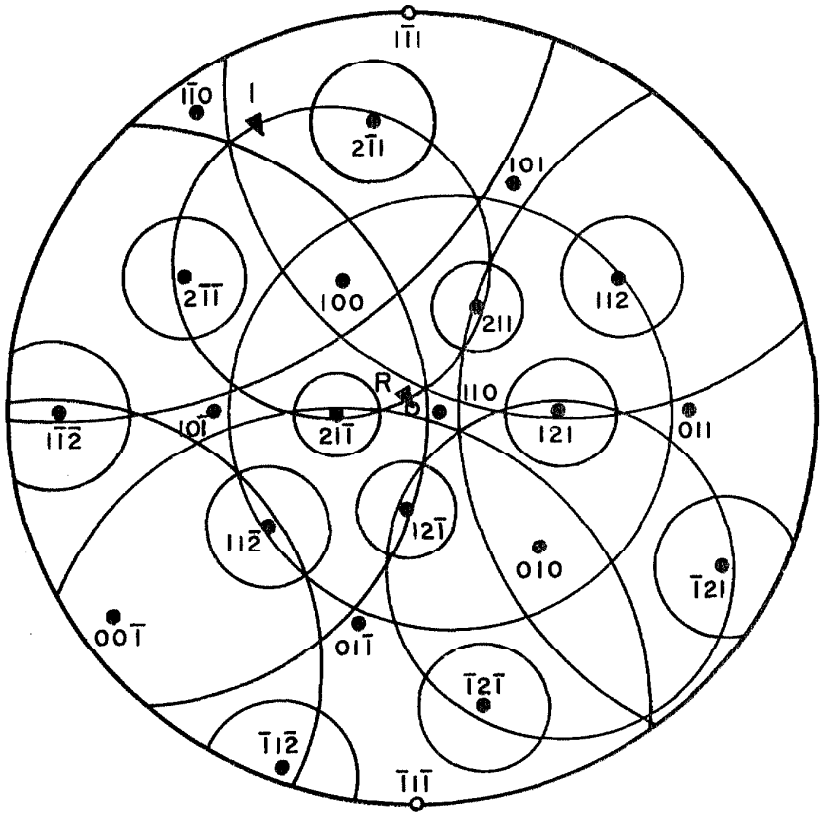

Figure 7. Reflection Locus Plot for Iron Crystal Illuminated with CrK_{α} Characteristic Radiation. Center of Plot is Normal to Specimen Observation Surface.

the projection are the loci of directions which satisfy the Bragg condition for the various sets of crystallographic planes and CrK_α radiation. All B-B topographs used for measuring dislocation motion in this study were made using the (200) planes as reflecting planes. The incident beam direction and the reflected beam directions are indicated by I and R respectively on the locus plot. Under these conditions, it is estimated that dislocations within approximately 3×10^{-4} cm of the free surface will be imaged on the B-B topograph.

Testing Sequence

After the final anneal, fresh dislocations were introduced by scratching the surface of the specimen. The scratching was done with a glass knife made by breaking a sheet of glass at a 90° angle. The load used on the knife was approximately 1 gm. The specimen was moved past the knife by a micrometer slide. A series of scratches 0.25 mm long separated by 0.12 mm gaps was made along the diameter of the specimen perpendicular to the $[1\bar{1}1]$ direction. After scratching, a B-B picture of the specimen was taken. This revealed the dislocation arrangement before the test. It was found that the scratch produced a furrow 1.25×10^{-3} cm wide. Slip bands extended 2.5×10^{-3} cm from the edge of the furrow, except where the knife was set down on the specimen. The slip bands were 2 to 3 times longer at these points.

For testing, the specimen was bonded between the torque transmission rods as shown in Figure 4. The bonding was done with Techkits A-12 epoxy resin cured for one hour at 100°C. In order to assure a continuous uniform bond on the scratched surface where dis-

location displacements were to be measured, a two-stage operation was used in making this bond. The specimen was first bonded to a teflon-covered rod. The epoxy was cured and the two pieces were separated. The pieces could be easily separated because the epoxy does not form a good bond with teflon. The revealed layer of epoxy resin was examined to make certain that it was continuous and free from bubbles. If the initial layer of the resin was found to be satisfactory, the specimen was bonded to the torque piece. The end of this torque rod which was adjacent to the scratched surface of the specimen was a disposable section of rod which was in turn bonded to the hexagonal section. The completed test specimen package was, as shown in Figure 4, the specimen and a disposable section of rod sandwiched between the two end pieces with hexagonal sections made to fit the sockets of the loading machine.

The specimen temperature during the test was controlled by immersing the torsion section of the loading machine in one of the following temperature baths:

373°K - glycerine heated by an electric heater controlled by a variable transformer,
295°K - room air,
198°K - methyl alcohol in equilibrium with solid CO_2,
77°K - boiling N_2.

The specimens were brought to temperature slowly. The maximum heating or cooling rate in all cases was 5°C per minute.

For tests at 198°K, 295°K, and 373°K, the load was applied by using the pulse loading capability of the load machine described above. At 77°K it was found that the epoxy resin had a tendency to break if

the load was applied with characteristic rise time of 3×10^{-2} sec. Therefore, the load was applied by bleeding pressure into the machine pressure chamber over a period of about 1 sec. Since the shortest test at $77^{\circ}K$ was 100 sec, the load rise time was a small percentage of the time at constant stress even for the slow application of the load.

After the test, the specimen package was disassembled in such a way that no stress was applied to the specimen. The disposable section of the torque rod was first cut through with an electric spark discharge cutting machine. The part of the disposable section which was still attached to the specimen was dissolved with 50% HNO_3. The specimen was protected from the acid by the epoxy layer over it. The epoxy resin was finally removed with Armstrong D-55 Stripper.

The above procedures were tested to see that they did not produce sufficient stress in the specimen to cause dislocation motion. For each temperature, the entire test sequence except for the application of the load was performed. Examination of B-B topographs taken before and after the sequence revealed no significant dislocation motion from the bonding process.

After the torque application rod had been removed from the tested specimens, the dislocation configuration was recorded by taking a B-B picture. The specimen was then polished for 10 - 15 sec in a solution of:

15 ml	30%	H_2O_2 ,
15 ml		H_2O ,
1 ml	50%	HF .

The polish was estimated to remove 5 - 10 μ of material from the surface. Another B-B topograph was taken after polishing. The purpose of polishing the specimen was to ensure that the dislocations would not be obscured by a slight corrosion which formed on the specimen from the epoxy stripper. The two after-test photographs were compared with the before-test photograph. Measurements were made from whichever picture showed the dislocations most clearly.

To summarize, the testing sequence consisted of the following operations:

1. Fresh dislocations were introduced by lightly scratching the surface.
2. A B-B picture was taken.
3. The specimen was bonded to the torque rod.
4. The test temperature was established.
5. The load pulse was applied.
6. The torque rod was removed by cutting the piece adjacent to the specimen, and then removing the remainder with nitric acid.
7. The epoxy resin was stripped from the specimen.
8. The after-test B-B picture was taken.
9. The specimen was lightly polished.
10. Another B-B picture was taken.

III. EXPERIMENTAL RESULTS

Dislocation Displacement and Position Measurements

After completion of a testing sequence, the before- and after-test B-B topographs were compared using a superposition comparison microscope (47). Dislocation displacements were determined by measuring the change in length of the slip bands which were produced by the scratch. Figure 8 shows a typical set of before- and after-test B-B photos. Measurements were made with a filar eyepiece attached to the microscope. The smallest division on the filar eyepiece, at the magnification used to make the measurements, is 8.0×10^{-5} cm. This distance is less than one tenth of the smallest dislocation displacement measured. Measurements were made for each slip band which had increased its length by an amount at least equal to its original length, except when the slip bands were in the vicinity of subgrain boundaries or damaged regions which were judged to have had an effect on the motion. In making the dislocation displacement measurements, the distortion of the B-B image of the crystal was ignored. Comparison of the size of the B-B image and the actual specimen dimensions indicates that neglecting this distortion resulted in overestimating the dislocation displacements by less than five percent.

As the slip band displacement measurements were made, the location of each measurement was marked on an enlargement of the B-B image. The position in the specimen of each slip band was then measured directly from the enlargement. The shear stress ($\tau_{\theta z}$) at each point where a displacement measurement was made was easily determined from its position. Using the approximation discussed in

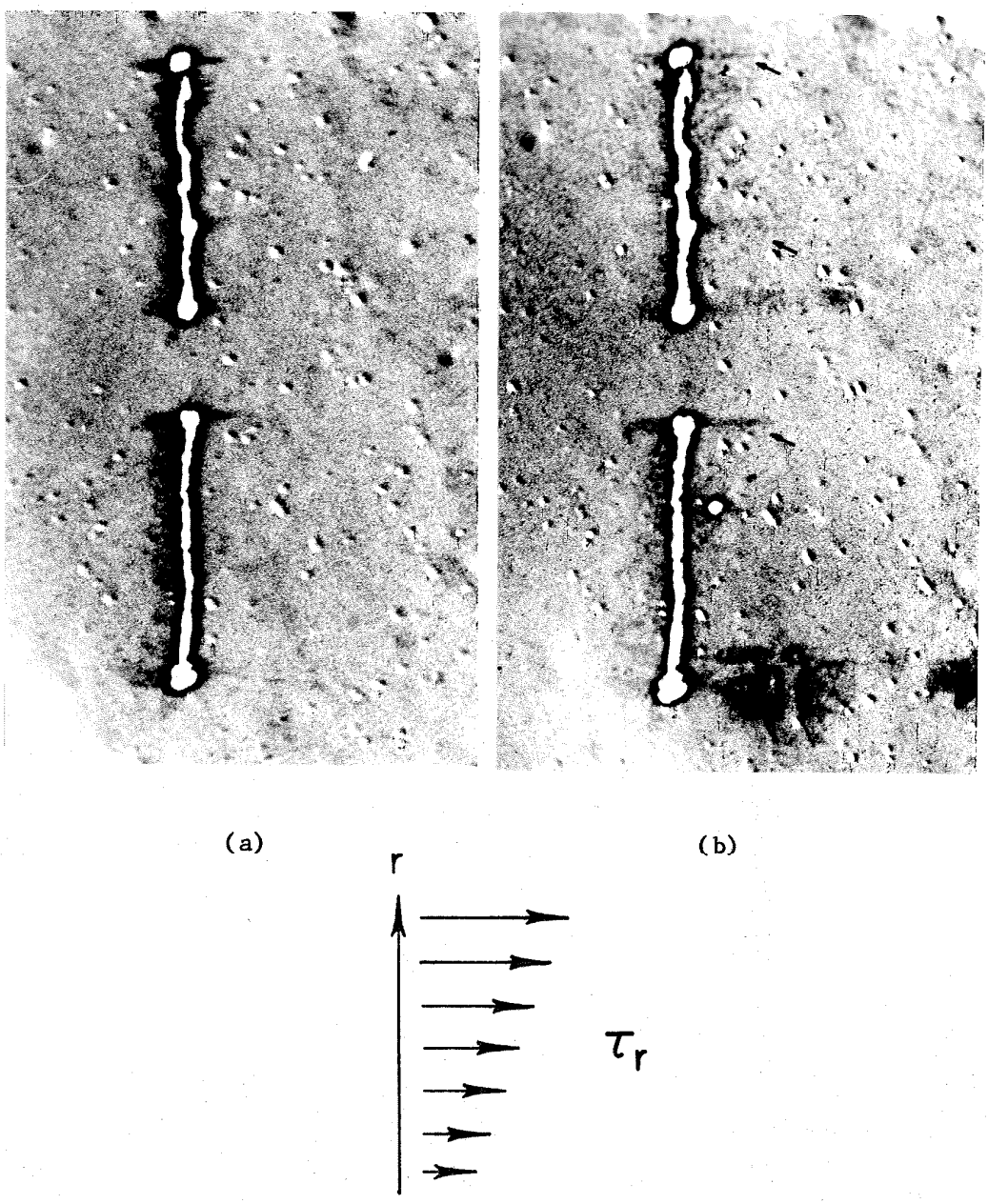

Figure 8. Typical Scratch Segment. (a) Before Application of Load Pulse. (b) After Loading. Direction of τ in Diagram is Direction of Force on Dislocation with Extra Half Plane Extending Toward Free Surface. Magnification 150X.

Section II that the stress state of the crystal is nearly the same as for an unconstrained single crystal rod in pure torsion, the stress state is given by:

$$\tau_{\theta z} = \frac{2Mr}{\pi r_o^4} \qquad \sigma_r = \sigma_\theta = \sigma_z = \tau_{r\theta} = \tau_{rz} = 0 \qquad [5]$$

Resolved Shear Stress

In order to determine the resolved shear stress on the dislocations, it is necessary to determine the Burgers vector and the slip plane of the dislocations for which displacement measurements were made.

Figure 9a shows a stereographic projection of the crystal centered on the normal to the surface of the specimen disc. The circles on the projection are the reflection locii for the (200), (121), (211), and (110) planes with CrK_α radiation. Also shown on the projection are the ⟨111⟩ Burgers vector directions. One of the Burgers vectors, $[1\bar{1}1]$, lies parallel to the crystal surface. For all test specimens, a scratch was made along the specimen diameter in the direction perpendicular to the $[1\bar{1}1]$ direction. This direction is indicated as the S_1 direction on the projection, and the relationship of the scratch to the Burgers vector is shown schematically in Figure 9b. This type of scratch was found to always produce only slip bands which had a surface trace of $[1\bar{1}1]$ as indicated in the figure. The application of stress caused these slip bands to become longer following the same trace.

Since the scalar product $\bar{b} \cdot \bar{n}$ for (200) reflections is the same for all Burgers vectors, this type of reflection cannot give any infor-

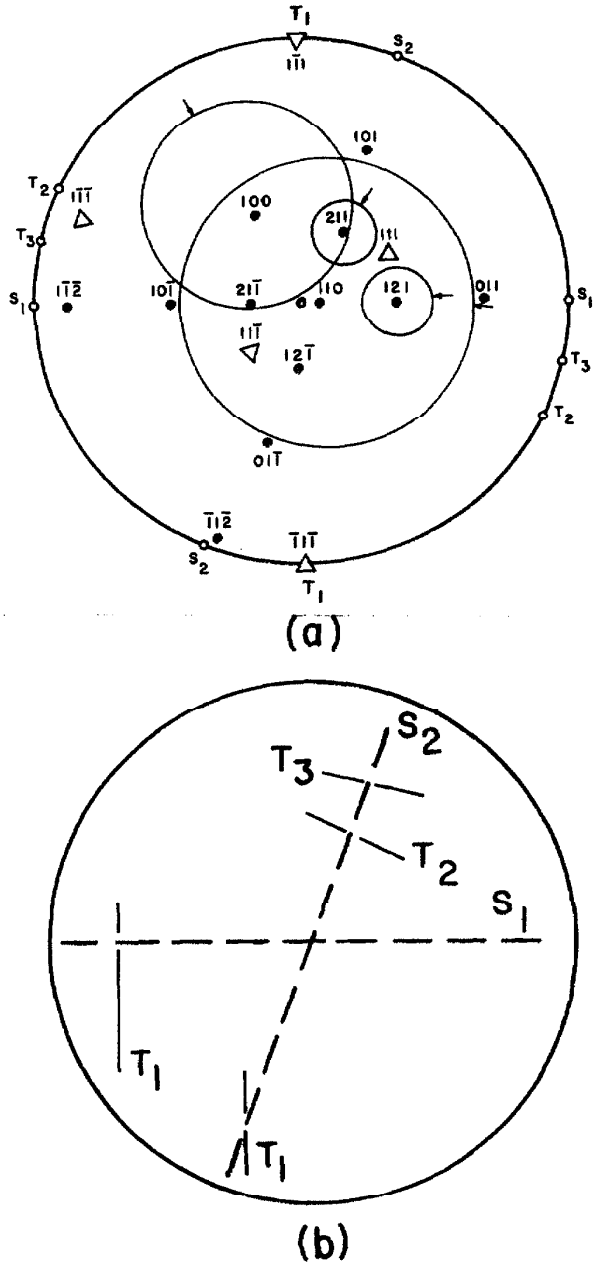

Figure 9. Observed Slip Bands. S - Scratch Directions; T - Slip Trace Directions. Possible Slip Planes {110} and {112}.

mation about the Burgers vector. Therefore, topographs of a specimen, scratched as described above, were taken before and after testing using the (200), (110), (121), and (211) planes as reflecting planes. The (200) type topographs confirmed the existence of slip bands as expected. The (110) topograph revealed some slip bands, but any additional displacement of these slip bands during the stress was undetectable. Furthermore, the areas of the specimen which contained many slip bands revealed in (110) topographs corresponded to areas where not much dislocation motion occurred, as observed in the (200) topographs. The (211) topograph revealed slip bands which increased their lengths during the stress pulse, while the (121) topograph revealed only a few slip bands which did not change their configuration during the stress pulse. These results indicate that the scratch in direction S_1 generates dislocations with several different Burgers vectors. However, the most predominant type of dislocation produced is that with the $1/2[1\bar{1}1]$ Burgers vector, and only dislocations with that Burgers vector undergo significant displacements during the stress pulse. This conclusion is consistent with the fact that the resolved shear stress is greatest on dislocations with the $1/2[1\bar{1}1]$ Burgers vector.

Because the slip trace and the Burgers vector are parallel for the dislocations measured, the slip plane cannot be determined from the slip bands produced by scratches of type S_1. Therefore, some specimens were also scratched in a direction perpendicular to the $[\bar{1}\bar{1}\bar{1}]$ direction. These scratches produced two or three types of slip bands. One type had traces parallel to the traces of the slip bands

produced by scratches of type S_1. The other families of slip bands had traces which corresponded closely to the traces of the (101) and $(01\bar{1})$ planes. After tests at 373°K, 298°K, and 77°K, no increase in length was ever detected in slip bands with trace T_2 or trace T_3. Small displacements were observed for some of the slip bands around the second scratch which had trace T_1. After testing and taking an 'after-test' photograph, the specimens were polished for 10 - 15 sec in a solution of H_2O_2 and HF of the composition listed in Section II. This was estimated to remove 5 - 10 μ of material from the specimen surface. A B-B topograph taken after the polish revealed many short lengths of dislocation extending out from the scratch S_2 for a distance of 50 - 80 μ. These observations strongly imply that the slip plane for dislocations which move is the (110) plane. Since this is also the most highly stressed plane, the resolved shear stresses were calculated on the basis of the slip plane being (110). The resolved shear stress (τ_r) on the dislocations in terms of the coordinate system shown in Figure 1 is:

$$\tau_r([1\bar{1}1],(110)) = \frac{2MY}{\pi r_o^3 R}\cos\phi \approx \frac{2MY}{\pi r_o^3 R} \qquad [6]$$

where r_o is the specimen radius measured on the specimen itself, Y is the coordinate of the dislocations along the scratch as measured on the enlargement of the B-B image, R is the radius of the enlarged image of the specimen. ϕ is the angle between the specimen normal and the [110] direction. The $\cos\phi$ term was set equal to unity in the calculations, since the values of ϕ for the test specimens were less than 10°. The resolved shear stresses for Figure 10 were calculated

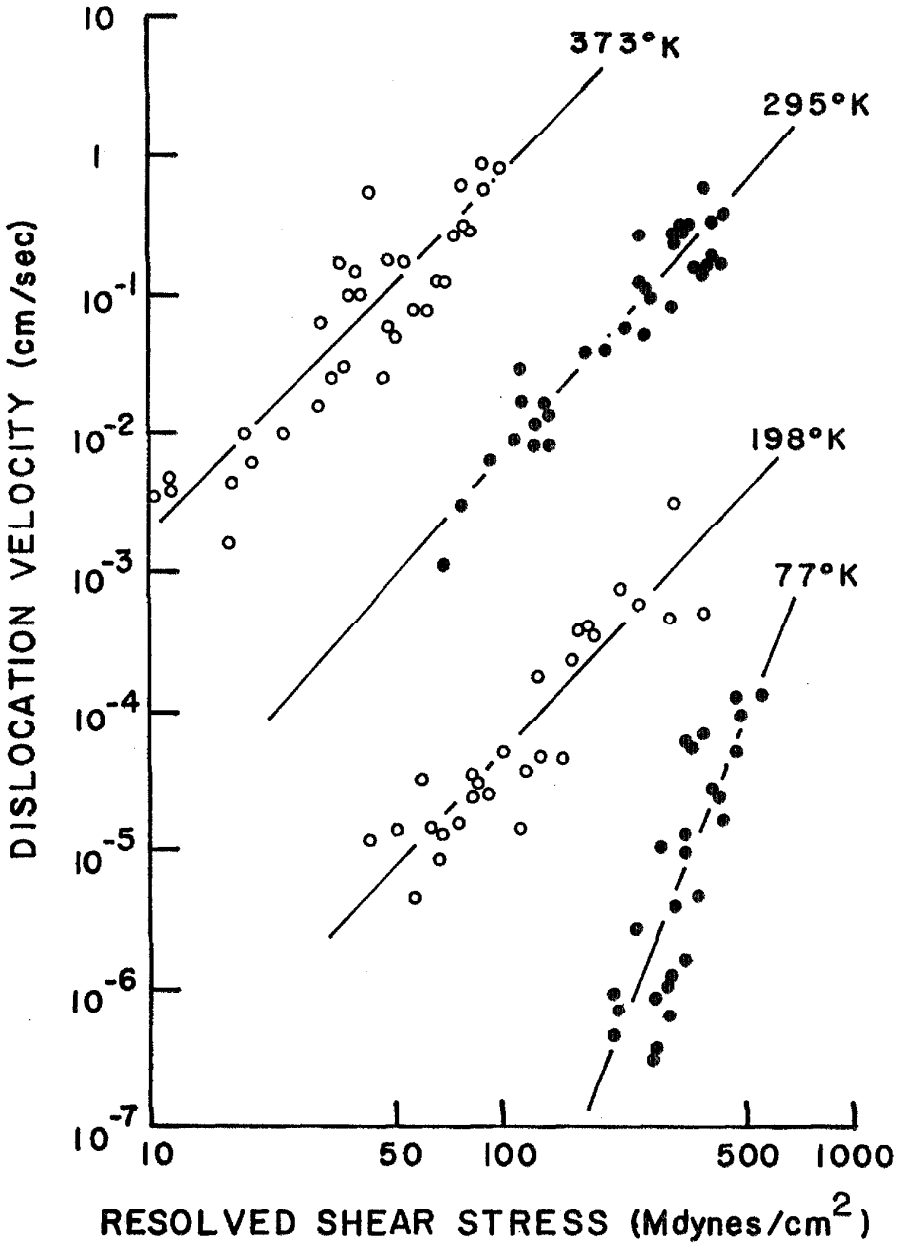

Figure 10. Dislocation Velocity in Iron Single Crystals as Function of Resolved Shear Stress for Several Temperatures.

from the dislocation positions using equation [6].

Dislocation Velocities

For all of the tests made below room temperature, the time for the stress to rise to its maximum value plus the time for unloading amounted to less than one percent of the time at constant stress. Therefore, for the low temperature tests, the total displacement was assumed to have taken place at constant stress. The average velocity of the dislocations was then computed by dividing the measured displacements by the time at constant stress. These velocities are plotted for 198°K and 77°K in Figure 10.

For some of the tests at room temperature and 373°K the time for loading plus unloading amounted to several percent of the time at constant stress, reaching as much as 150 percent on some tests at 373°K. Therefore, the following analysis was used to remove the effect of the pulse rise time from the calculated velocities. For the first approximation of the velocity, the rise and fall times were neglected and the velocity was computed to be the displacement divided by the time at constant stress. Since the relationship between the logarithm of the velocity and the logarithm of the stress seemed to be linear, the data were assumed to be adequately described by

$$v = v_o(\tau/\tau_o)^m \qquad [7]$$

over the range for which measurements were made. Where v is the dislocation velocity, v_o is 1 cm/sec, τ is the resolved shear stress, τ_o is the stress necessary to produce a velocity of 1 cm/sec, and m is a dimensionless constant. A least squares analysis was used to

determine the values of m and τ_o which would best fit the logarithms of resolved shear stress and velocity to the linear relationship

$$\ell n\, v/v_o = m\, \ell n \tau - m\, \ell n \tau_o . \qquad [8]$$

The stress pulse was then approximated by a trapezoid described by:

$$\tau(t) = \begin{cases} \tau_c(t/t_1) & 0 \le t \le t_1 \\ \tau_c & t_1 \le t \le t_2 \\ \tau_c\left(1 - \dfrac{t-t_2}{t_3-t_2}\right) & t_2 \le t \le t_3 \end{cases} \qquad [9]$$

where τ_c is the stress during the constant part of the pulse. The total displacement can then be calculated by integrating the velocity given by equation [7] over a stress pulse given by [9]. The resulting displacement is given by the formula

$$D = D_1 + D_2$$

$$D = v_o\left(\frac{\tau_c}{\tau_o}\right)^m \left(\frac{t_1+t_3-t_2}{m+1}\right) + v_o\left(\frac{\tau_c}{\tau_o}\right)^m (t_2-t_1) \qquad [10]$$

where the first term represents the displacement which occurred during the rise and fall of the pulse and the second term represents the displacement during the constant part of the pulse. Since the first approximation used for the velocities was $v' = D/(t_2-t_1)$, the velocities were over-estimated and should be reduced by a factor of:

$$v/v' = \frac{D_2}{D} = \frac{(t_2-t_1)(m+1)}{(t_1+t_3-t_2)+(m+1)(t_2-t_1)} . \qquad [11]$$

Thus, by using equation [11], a new set of approximations for the velocities was obtained. Then a new least squares fit was made for the corrected velocities. This yielded a new value for m which enabled recalculation of the corrected velocities. The process was iterated

until the largest change in velocity between iterations was less than one percent. The difference between initial and corrected velocity was as large as 30 percent for the shortest test at 373°K. The values plotted in Figure 10 are the corrected values of the velocities. Table 1 gives the values of m and τ_o for the best fit to the form of equation [7], both before and after the corrections were made on the velocities.

TABLE I

Dislocation Mobility Parameters in Iron

Temperature	Mobility Parameters			
(^{o}K)	m	τ_o (Mdynes/cm^2)	m†	τ_o† (Mdynes/cm^2)
373	2.56 ± 0.5	119 ± 10	2.76	100
295	2.83 ± 0.5	589 ± 60	2.87	576
198	2.61 ± 0.5	4080 ± 1000		
77	6.25 ± 0.5	2240 ± 500		

† Quantities marked † were calculated before correction for the rise time.

IV. DISCUSSION

Experimental Errors

The wide scatter of the data indicates that there are sizeable random errors associated with these experiments. Such errors are probably associated with irregularities in the stress and differences in dislocation configuration at various points in the specimen. Part of the scatter arises from uncertainty in determining the ends of the slip bands. Although the width of the scatter bands of data makes it difficult to evaluate the degree of the agreement between these experimental results and the fine points of various theories, purely random variations would not invalidate the trends observed in these experiments.

Of more fundamental interest is the possibility of systematic errors in the experiments which could bias the results sufficiently to lead to incorrect conclusions. There are two important sources of systematic error in these experiments:

1. pile-up effects in the slip bands;
2. stress concentration introduced by the scratch.

Both of these effects could mean that the actual stress acting on the dislocations was greater than the nominal applied stress.

Because measurements were made on slip bands instead of on individual dislocations, there is a possibility that the stress acting on the leading dislocation was enhanced by the stress fields of the trailing dislocations. It was impossible to establish the dislocation content of the slip bands observed in this investigation because the B-B topographs did not resolve the slip bands into individual dislocations.

However, in an investigation of Fe-3°/o Si alloy single crystals by the etch pitting technique, Stein and Low (6) were able to establish that a slip band consisted of a single dislocation loop which left many smaller loops in its wake as it moved away from the scratch. Presumably such loops are the debris left behind from cross slip of screw segments of the dislocations or from interaction of the moving dislocation with other dislocations and obstacles. Since such loops have no long range stress fields, they exert no force on the moving dislocation after it leaves them behind. If the slip bands observed in the present investigation were similar to those in Fe-3°/o Si, then the velocity of the leading dislocation would not have been enhanced by stress fields from the trailing dislocations, but would in fact have been decreased by the athermal drag associated with the formation of the loops of debris.

The possibility still remains that the slip bands in the pure iron crystals used here were composed predominantly of dislocations of one sign. The difference between the behavior of the leading dislocation in such a pile-up and that of an isolated dislocation should be considered. Fortunately, this question has been treated theoretically by Rosenfield and Hahn in their computer simulation of the motion of many dislocations emitted from a single source (48). The assumptions of the Rosenfield and Hahn analysis are that the velocity stress relationship for the dislocations can be approximated over the range of interest by the form:

$$v = Ce^{B\tau} \qquad [12]$$

and that a new mobile dislocation is generated by the source each

time that the total stress on the source dislocation reaches a value τ_s. Solving for the position of the leading dislocation as a function of time as the source continued to emit dislocations, they found that the lead dislocation reached a terminal velocity after only five or six dislocations had been emitted from the source. The effective stress (τ_e) associated with the terminal velocity, in terms of the source activation stress (τ_s) and the applied stress (τ_a), is given by:

$$\tau_e = \tau_a + \frac{3}{4}(\tau_a - \tau_s) \quad . \qquad [13]$$

When the source stress is much less than the applied stress,

$$\tau_e = 1.75\,\tau_a \quad . \qquad [14]$$

For a velocity stress relationship of the form:

$$v = Ce^{B\tau} = v_o e^{\frac{-(U_o - bA\tau)}{kT}} \quad , \qquad [15]$$

neglecting the pile-up effect in a slip band composed of dislocations of like sign results in over-estimating the activation area (A) by 75 percent. For the formulation

$$v = v_o(\tau/\tau_o)^m \quad , \qquad [16]$$

the error is 75 percent in the value of τ_o. It should be noted that these errors are essentially constant for all slip bands containing more than ten dislocations. Therefore, even if the slip bands in this investigation were composed of dislocations of a single sign, the conclusions would be substantially the same except for a factor of 1.75 in the magnitude of A or τ_o.

The magnitude of the error introduced by the stress concentration around the scratch can be approximately evaluated from the

data. In many cases at 373°, 295°, and 198°K, measurements were made for nearly the same stress on two different tests of different duration and different maximum load. It is therefore possible to compare velocities derived for a stress based on measured displacements which differ by as much as an order of magnitude. Table II gives several examples of such comparisons. Also given for purposes of comparison are several cases where several measurements were made for the same stress with comparable pulse durations. As shown in Table II, there appears to be little systematic deviation of the velocities derived from small displacements from those derived from large displacements. It is thus concluded that at 373°, 295°, and 198°K, the effect of the stress concentration near the scratch is small compared to the width of the data scatter bands.

For the tests at 77°K the stress sensitivity of the velocity was so great that displacements could only be measured on a small portion of the specimen. Therefore, in tests which showed measurable displacements only at the outer edge of the specimen, it was impossible to be certain that all observed motion was not associated with stress concentrations. In order to disprove this possibility, three tests were conducted at a maximum stress level near 600 Mdynes/cm^2 for durations of 100, 1000, and 10000 sec , respectively. The 100 sec test produced measurable displacements only at the outer radius of the specimen. The 1000 and 10000 sec pulses produced measurable displacements successively further in on the radius and very large displacements which could not be measured in the region outside of the measurable region. This, along with the consistency of the data,

TABLE II

Typical Stress-Displacement-Velocity Data for Tests of Different Durations

Temperature (^{o}K)	Duration of Pulse (sec)	Stress (Mdynes/cm^{2})	Displacement (cm)	Velocity* (cm/sec)
373	0.95	35.8	2.87×10^{-2}	2.96×10^{-2}
	0.027	30.8	2.48×10^{-3}	6.04×10^{-2}
	0.025	50.4	1.68×10^{-3}	4.71×10^{-2}
	0.030	53.7	7.60×10^{-3}	1.78×10^{-1}
	0.030	47.0	7.50×10^{-3}	1.77×10^{-1}
295	5.12	138	7.73×10^{-2}	1.41×10^{-2}
	0.30	138	2.82×10^{-3}	0.92×10^{-2}
	0.35	254	1.00×10^{-1}	2.81×10^{-1}
	0.30	250	3.92×10^{-2}	1.28×10^{-1}
	0.10	259	1.22×10^{-2}	1.16×10^{-1}
	0.10	255	5.68×10^{-3}	5.40×10^{-2}
198	600	58.8	2.02×10^{-2}	3.37×10^{-5}
	600	58.0	2.72×10^{-3}	4.53×10^{-6}
	193	63.8	2.96×10^{-3}	1.53×10^{-5}

* The velocities for 373^{o} and 295^{o}K have been corrected for the rise time of the pulse.

is considered adequate evidence that stress concentration effects play a no more important role at 77°K than in the tests at higher temperature.

Theoretical Predictions

The strong temperature dependence of the dislocation velocity at constant stress clearly indicates that a thermally activated process is important in determining the mobility of dislocations in iron in the temperature range covered by this investigation. Therefore, a detailed consideration of the assumptions and predictions of the Peierls and interstitial impurity mechanisms is in order.

Many authors (16 - 20, 49 - 51) have considered the process of thermal activation of dislocations over the Peierls energy barriers. All of the models are based on the same basic idea but differ in the assumptions made in order to simplify the exact problem. The basic premise of the Peierls theories is that because of the periodicity of the lattice, the core energy and therefore the total line energy of the dislocation varies with the position of the dislocation in the lattice:

$$\Gamma(y) = \text{periodic function of } y \, . \qquad [17]$$

The drag stress exerted on the dislocation is then:

$$\tau_d = \frac{1}{b}\left[\frac{\partial \Gamma(y)}{\partial y}\right] \quad , \qquad [18]$$

which has a maximum value usually called the Peierls stress (τ_p);

$$\tau_p = \max\left[\frac{1}{b}\left(\frac{\partial \Gamma(y)}{\partial y}\right)\right] \, . \qquad [19]$$

When the applied stress (τ_a) is less than the Peierls stress (τ_p), the dislocation cannot move except when aided by the thermal fluctuations of the lattice.

The nature of the thermal activation process is that a critical length of the dislocation is moved by thermal fluctuation over the Peierls barrier as in Figure 11. The critical configuration for the activated segment is defined as the configuration for which the energy of the dislocation minus the work done by the applied stress is a maximum. Therefore, once the critical configuration is reached, the applied stress can drive the two kinks apart, causing an entire length (L) of the dislocation to move forward the distance between Peierls energy minima. This distance is either equal to $\bar{b}$, the Burgers vector, or simply related to it by the lattice geometry. For simplicity, the distance moved per activation will be assumed to be $\bar{b}$ for the remainder of this discussion. The equation for the velocity of a dislocation then becomes:

$$v = v_o \exp\left(\frac{-U(\tau_a)}{kT}\right) = b\nu \exp\left(\frac{-U(\tau_a)}{kT}\right) \qquad [20]$$

where ν is the attempt frequency, and the product of ν with the exponential is the frequency of successful attempts.

The differences between the various calculations based on this thermal activation model arise from the assumptions made about the critical kink configuration and the estimation of the attempt frequency. Of the many contributions to the literature concerning the thermal activation of dislocations over the Peierls energy barrier, those by Seeger (16), Friedel (19), and Dorn and Rajnak (20) will be considered here. These three papers are representative of the various different approaches and are also the ones most often cited in the literature.

Seeger's model is based on an assumed critical configuration

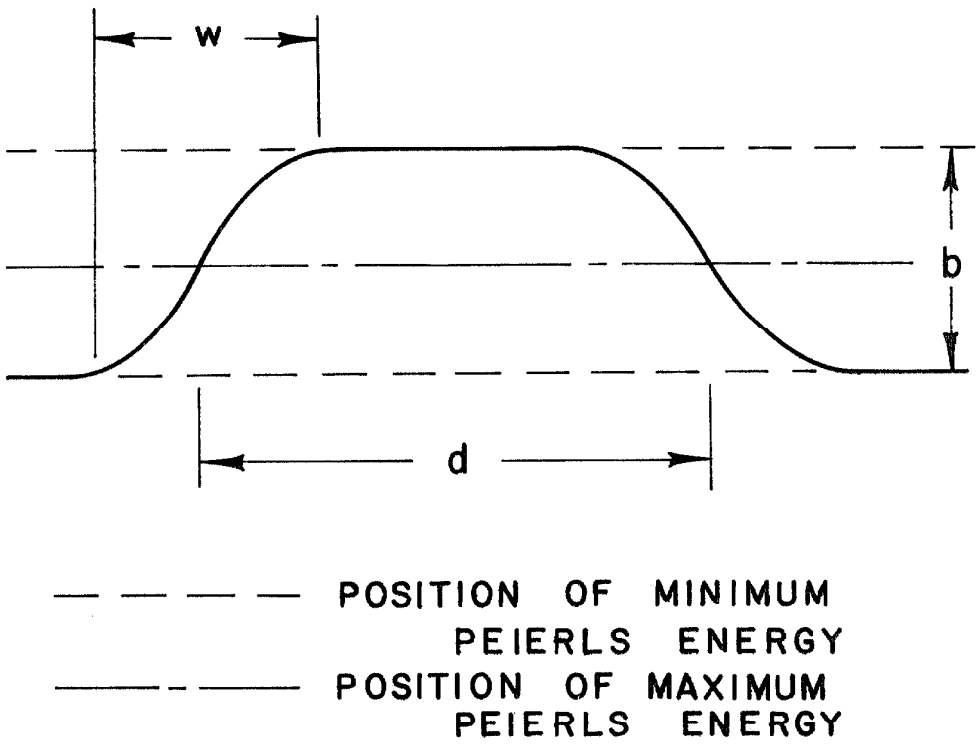

Figure 11. Schematic Diagram of Double Kink in Dislocation.

as shown in Figure 12a. Two half kinds a distance (d) apart are joined by a segment of dislocation which lies at the top of the energy barrier. The distance between the two half kinks at the critical point is such that the force exerted on the kinks by the applied stress is equal to the force of attraction between the two kinks. For sufficiently small stresses, the critical spacing is large compared to the kink widths (w). For this case, the force of attraction between the kinks can be calculated. With the additional assumption of a sinusoidal Peierls potential barrier, the activation energy for a critical activated segment can be expressed in closed form. The expression for this activation energy is given in Table III. This model predicts that the activation energy is proportional to the logarithm of the stress. The attempt frequency (ν) is taken by Seeger to be the vibrational frequency of a rigid dislocation lying in the Peierls potential valley. The resulting expression for v_o is given in Table III.

The Friedel model is based on a different critical configuration. Friedel argues that because the line energy of a dislocation is so large, the kinks must be very wide. Therefore, he assumes the critical configuration to be the triangular form shown in Figure 12b. Furthermore, he assumes that since the slopes of the kinks are so small, the interaction between the kinks can be neglected except for cases when ℓ is of the order of b. A sinusoidal form of the Peierls barrier is assumed. The energy of the assumed kink configuration can be calculated as a function of the length (ℓ) of the kink. The energy has a minimum for a critical kink length (ℓ_o) which is related to the applied stress by:

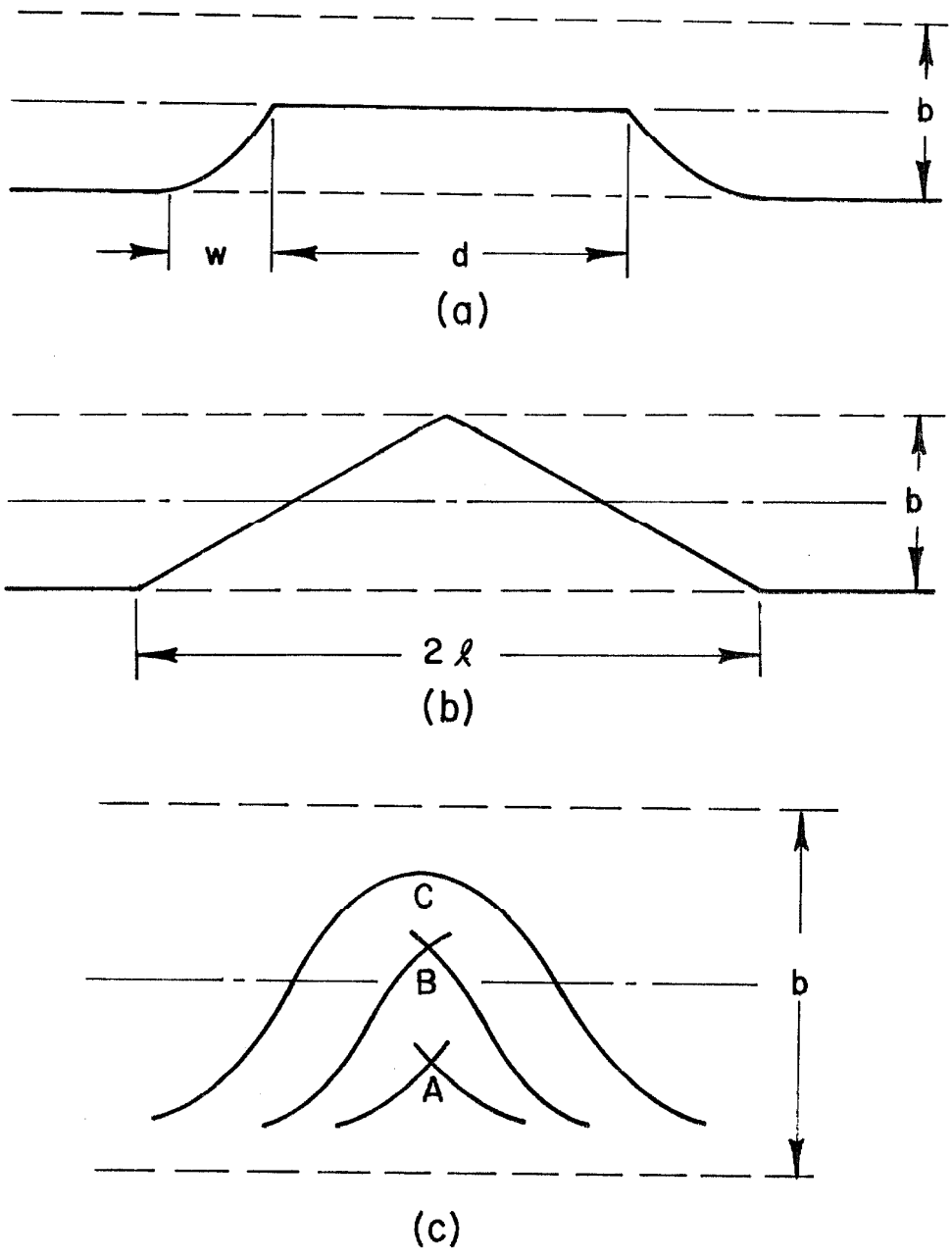

Figure 12. Proposed Critical Double Kink Configurations. (a) Seeger, (b) Friedel, (c) Dorn and Rajnak.

TABLE III

Comparison of Peierls Models

Activation Energy

Seeger	$\frac{2b}{\pi}\left(\frac{2\Gamma_o b^2 \tau_p}{\pi}\right)^{\frac{1}{2}}\left(1+\frac{1}{4}\ell n\left(\frac{16\tau_p}{\pi\tau_a}\right)\right)$
Friedel	$2b^2\left[\tau_p\left(1-\frac{\tau_a}{\tau_p}\right)\right]^{\frac{1}{2}}$
Dorn and Rajnak	cannot be expressed in closed form; see Figure 13.

Activation Volume $(-\partial U/\partial \tau_a)$

Seeger	$\frac{b}{2\pi}\left(\frac{2\Gamma_o b^2 \tau_p}{\pi}\right)^{\frac{1}{2}}\frac{1}{\tau_a}$
Friedel	$\frac{b^2\Gamma_o^{\frac{1}{2}}}{(\tau_p-\tau_a)^{\frac{1}{2}}}$
Dorn and Rajnak	cannot be expressed in closed form: see Figure 14.

Pre-exponential Term (v_o)

Seeger	$v_s b\left(\frac{\tau_p}{2\pi}\right)^{\frac{1}{2}} \approx 1.4\times 10^4$ cm/sec v_s = shear wave velocity
Friedel	$\frac{\sqrt{\pi}}{16} L^2 b \nu_D\left(\frac{kT(\tau_p-\tau_a)^5}{\Gamma_o^7}\right)^{\frac{1}{2}} \approx 6\times 10^8$ cm/sec ν_D = Debye frequency L = free length of the dislocation

TABLE III (continued)

Dorn and Rajnak	$\nu_D b(\frac{L}{d}) \approx 10^3$ cm/sec d = length of the double kink
Fleischer (impurity hardening)	$v_o \approx 2 \times 10^8$ cm/sec

The numerical values for v_o are given for: $L = 10^{-4}$ cm , $T = 150^oK$, $\nu_D = 8.75 \times 10^{12}$ sec^{-1} , $\Gamma_o = Gb^2$.

$$\ell_o = \left(\frac{\Gamma_o}{\tau_p - \tau_a}\right)^{\frac{1}{2}} . \qquad [21]$$

The expressions for the activation energy and v_o derived from this model are given in Table III. This model neglects the interaction between the kinks, so it is probably not valid for small stresses where ℓ_o becomes small. As τ_a approaches τ_p the length of the kink becomes very large. Therefore, this model would require cooperative motion of many atoms at high stresses. This probably means that the usefulness of this approximation is limited to medium stresses where ℓ_o is of the order of ten to several hundred b.

The model of Dorn and Rajnak begins with the same sort of line energy approach used in the Friedel model. However, instead of assuming a shape for the critical kink, Dorn and Rajnak used a variational principle to calculate the lowest energy shape of a kink as it is formed. The calculated kink configurations are shown in Figure 12c. Curves A and B represent unstable kinks which will decay and disappear after the thermal fluctuation passes. Curve C represents the saddle point configuration where the slope of the dislocation line at the center of the double kink first becomes continuous. Curve C then represents the critical kink configuration. After a double kink reaches shape C, it can dissociate into single kinks which move apart under the action of the applied stress. The activation energy for the formation of the critical kink is the excess energy of a dislocation in configuration C over a straight dislocation lying in the Peierls valley. This energy cannot be expressed in closed form, but it is compared graphically with the activation energy of the Friedel model in Figure 13.

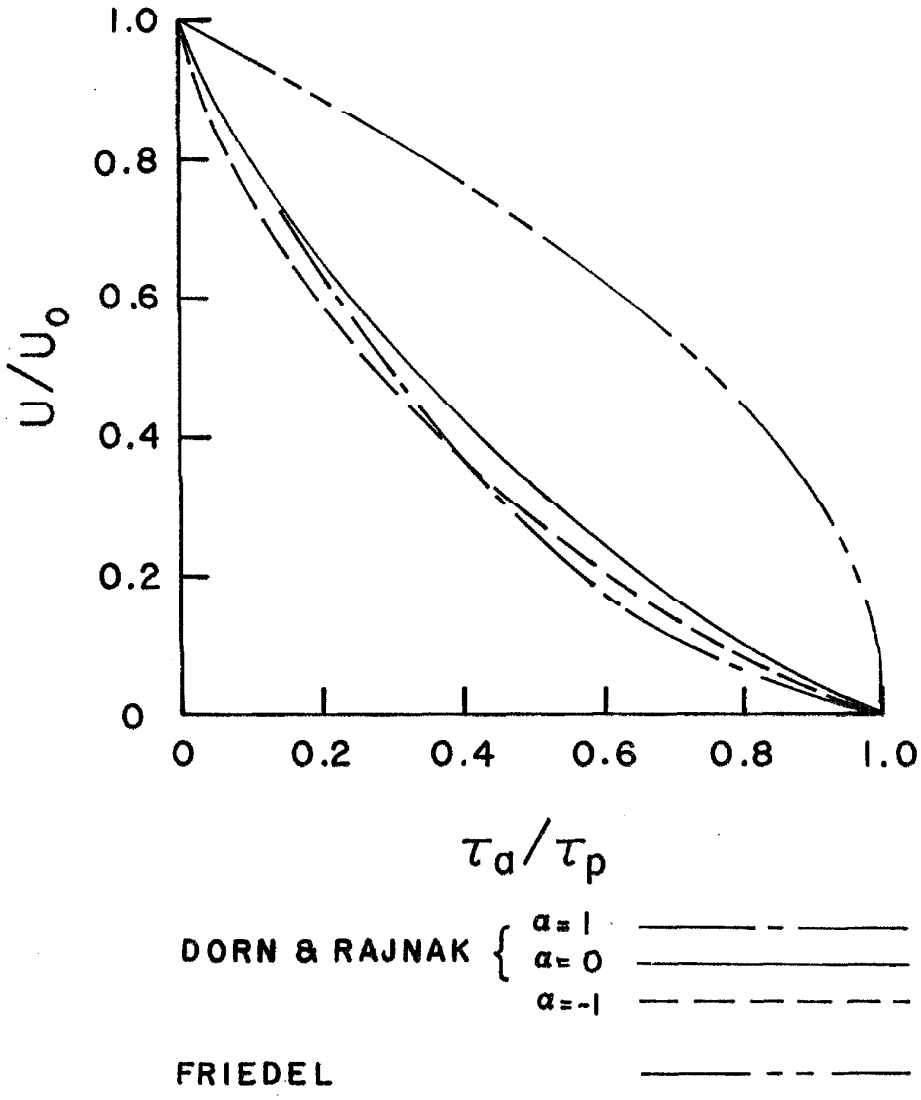

Figure 13. Activation Energy as Function of Applied Stress for Some Peierls Mechanisms.

The expression which Dorn and Rajnak give for v_o in the case where the velocity of a kink is large is given in Table III.

The assumptions and limitations of the three models can be summarized in the following way. Both the Seeger and Friedel models begin with an assumed kink configuration. Seeger derives the critical kink spacing by balancing the force from the applied stress against the interaction force between the two kinks. Friedel assumes that only the line energy of the kinked dislocation is important, and ignores the attraction between the kinks. Dorn and Rajnak improve upon the other two theories by deriving an expression for the critical kink shape. However, Dorn and Rajnak like Friedel ignore the interaction of the kinks. Friedel and Seeger both ignore the fact that when an applied stress is acting on the dislocation, it does not lie at the bottom of the Peierls potential valley but has been moved partially up the barrier. An additional refinement of the Dorn and Rajnak model is that it includes this effect. Both the Seeger and Friedel models appear to break down for very small and very large stresses. The Dorn and Rajnak model, since it involves fewer assumptions, is probably applicable over a wider range of applied stress.

Calculations of the activation energy from any of the expressions in Table III or from Figure 13 require that the Peierls stress be known. Since estimations of the Peierls stress range over many orders of magnitude, the values of measured activation energy cannot be used as suitable checks on the above theories. The most noticeable difference between the various theories is in their predictions of the effect of applied stress on the activation energy. The differences in

the partial derivatives of the activation energy with respect to applied stress can be seen in Figure 14 and the expressions in Table III. This quantity has units of volume and is usually referred to as activation volume. The activation volume defined in this way can roughly be associated with the product of the Burgers vector and the area swept out by the dislocation during the activation process. However, this correspondence is exact only if the activation energy has the form:

$$U = U_o - V\tau_a \quad , \qquad [22]$$

where U_o and V are constants.

The question of temperature dependence of the activation energy has not been answered with any degree of certainty. A small temperature dependence is included implicitly through Γ_o in all theories, since Γ_o is proportional to the shear modulus (G) which is temperature dependent. The shear modulus decreases 5 - 10 percent as the temperature increases from 77 - 373°K. An additional temperature dependence can be included if the height or the shape of the Peierls barrier is affected by temperature. This sort of change was calculated by Kuhlman-Wilsdorf (52) to cause the Peierls stress to change with temperature as:

$$\tau_p = \tau_k \exp(-T/T_M) \quad , \qquad [23]$$

where T_M is the melting temperature and τ_k is the Peierls stress at zero degrees Kelvin. Seeger (17, 53), by considering the quantum mechanical partition functions of the activated and unactivated dislocation, has found that the activation energy decreases logarithmically as the temperature decreases. However, he believes the magnitude

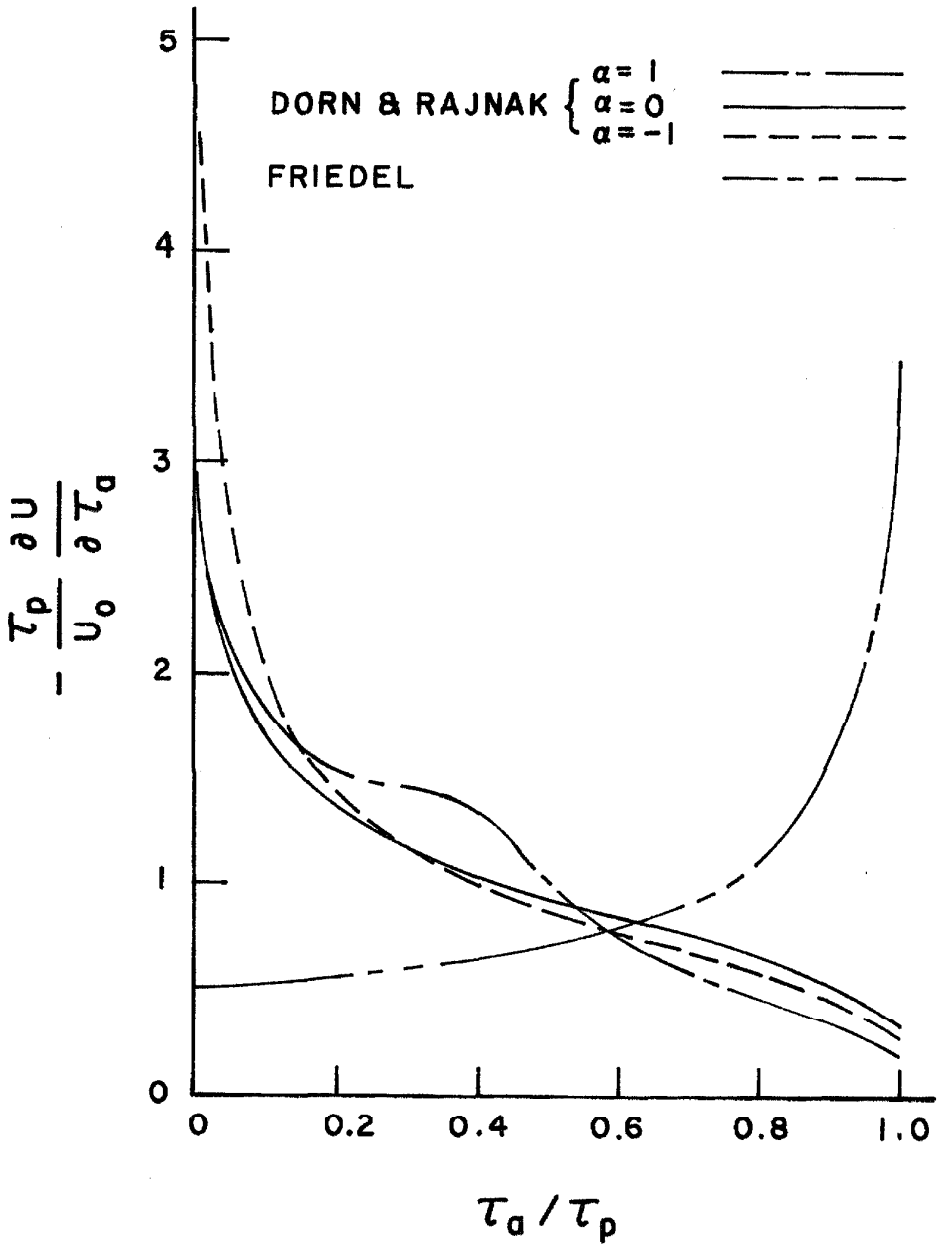

Figure 14. Activation Volume as Function of Applied Stress for Some Peierls Mechanisms.

of the effect to be small. Finally, the above theories deal only with the enthalpy of activation. This means that the entropy term in the free energy has been neglected. All authors agree that some increase in entropy should be associated with the formation of kinks. However, this term is difficult to treat theoretically and is therefore usually ignored.

The pre-exponential term (v_o) may also change with temperature. Since the theoretical estimations of this term are quite crude, the question of temperature dependence is ignored. The usual argument given is that any change in v_o with temperature would be small compared to the exponential term.

Fleischer (13, 14) has proposed that the mechanism which controls the motion of dislocations in BCC metals is the thermal activation of the dislocations past the stress fields of interstitial impurity atoms. Interstitial atoms in the BCC lattice produce tetragonal strain. This strain field interacts strongly with the stress field of the dislocations. Consequently, when a dislocation approaches an impurity atom near its slip plane, a large force is exerted on the dislocation. For impurities within a few b of the slip plane, the interaction is so strong that the dislocation cannot be moved past the impurities by the applied stress alone. Considering the impurities in the two atomic planes bordering the slip plane, Fleischer's model gives the activation energy to be:

$$U = F_o b[1 - (\tau/\tau_c)^{\frac{1}{2}}]^2 \qquad [24]$$

$$F_o = G\Delta\epsilon b^2/3.86\,\beta \qquad [25]$$

where $\beta = 1$ for screw dislocations, $\beta = 1-\nu$ for edge dislocations,

and $\Delta\epsilon$ is the difference between the longitudinal and the transverse strains of the distortion. $\Delta\epsilon$ equals 0.41 for carbon in iron (13). τ_c is the stress required to move the dislocations past the impurities at $0^{\circ}K$ and is given by:

$$\tau_c = (F_o/bL) \ . \qquad [26]$$

L is the average distance between impurities adjacent to the slip plane and is given in terms of the concentration of impurity atoms by:

$$L = b/(2c)^{\frac{1}{2}} \ . \qquad [27]$$

If ν_L is the vibrational frequency of a dislocation length L, then the dislocation velocity is:

$$v = \nu_L L \exp(-U/kT) \ . \qquad [28]$$

The normalized activation energy and its derivative with respect to applied stress are shown in Figures 15 and 16.

This theory, unlike the Peierls theories, is well-defined in terms of independently measurable quantities such as the impurity content and the tetragonal distortion produced by the interstitial atoms. There are, however, two weaknesses of calculations based on this theory. First, the theory does not properly take into account the fact that the obstacles are a random dispersion instead of a uniform network. Second, the important interactions in this theory are the ones where the dislocation approaches the impurity so closely that linear elasticity can no longer be applied to the calculation of the interaction energy. However, it is difficult to imagine the uncertainty of the quantities in the impurity theory being greater than an order of magnitude. This is a small degree of uncertainty when compared

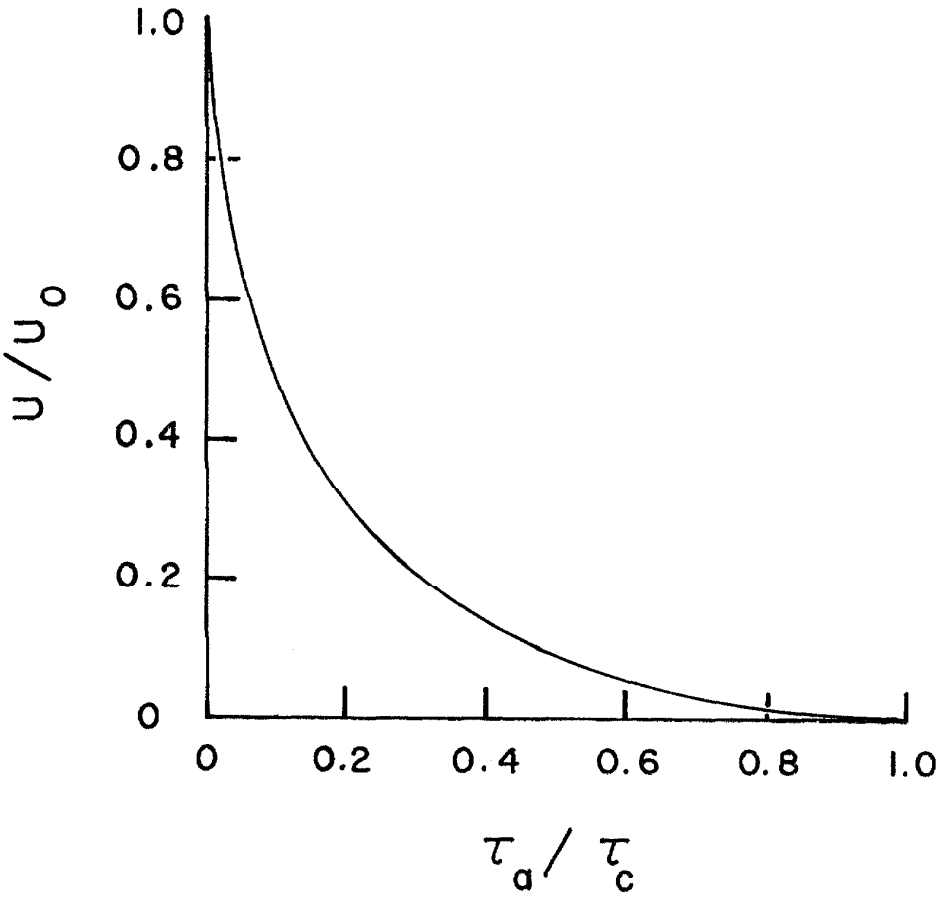

Figure 15. Activation Energy as Function of Applied Stress for Impurity Hardening Model.

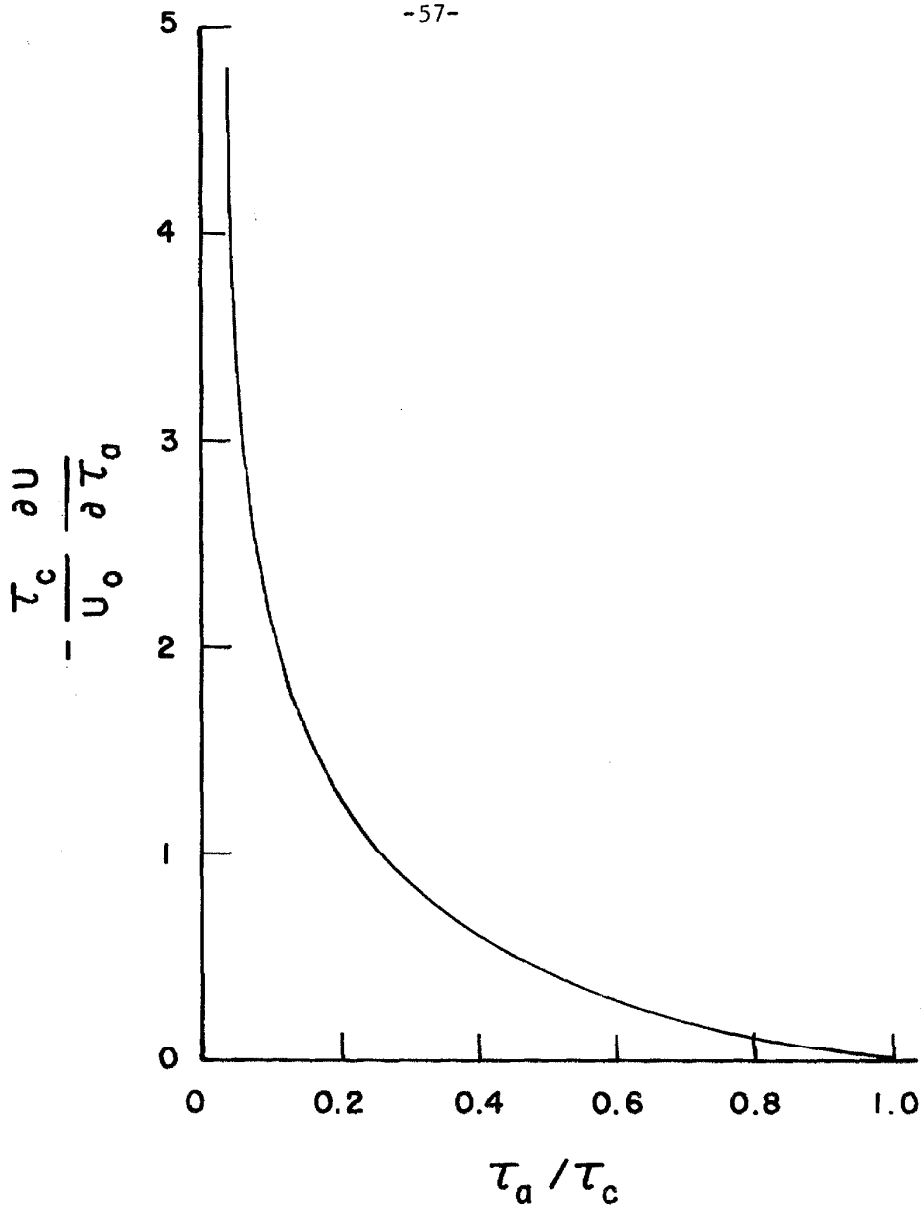

Figure 16. Activation Volume as Function of Applied Stress for Impurity Hardening Model.

with the uncertainty in calculations of the Peierls stress.

Comparison of Experimental Results with Theoretical Predictions

The above theories all predict that the dislocation velocity is related to stress and temperature by an equation of the form:

$$v = v_o \exp\left(\frac{U(\tau_a)}{kT}\right) . \qquad [29]$$

This indicates that the data might be more properly presented with the logarithm of the velocity plotted against linear stress than as they are presented in Figure 10. Therefore, the experimental data have been replotted in that way in Figure 17.

The thermal activation theories all assume that v_o and U are either independent of temperature or only very weak functions of temperature. This leads immediately to the conclusion that:

$$\left(\frac{\partial \ell n\, v/v_o}{\partial\, 1/T}\right)_\tau = \frac{-U}{k} = \text{constant.} \qquad [30]$$

However, Figure 18 clearly shows that the logarithm of the dislocation velocity is not linearly related to the reciprocal of the temperature for constant stress. Furthermore, it does not appear that the experimental results can be explained by a simple addition of two thermally activated mechanisms occurring simultaneously. Lines A and B in Figure 19 represent the predicted velocity lines for two thermally activated mechanisms acting independently. If both processes were occurring simultaneously in a material, the predicted velocity curve would be similar to the dashed line in Figure 19. When the velocity for one process is much less than for the other, the slower mechanism will predominate. Where the velocities of the two

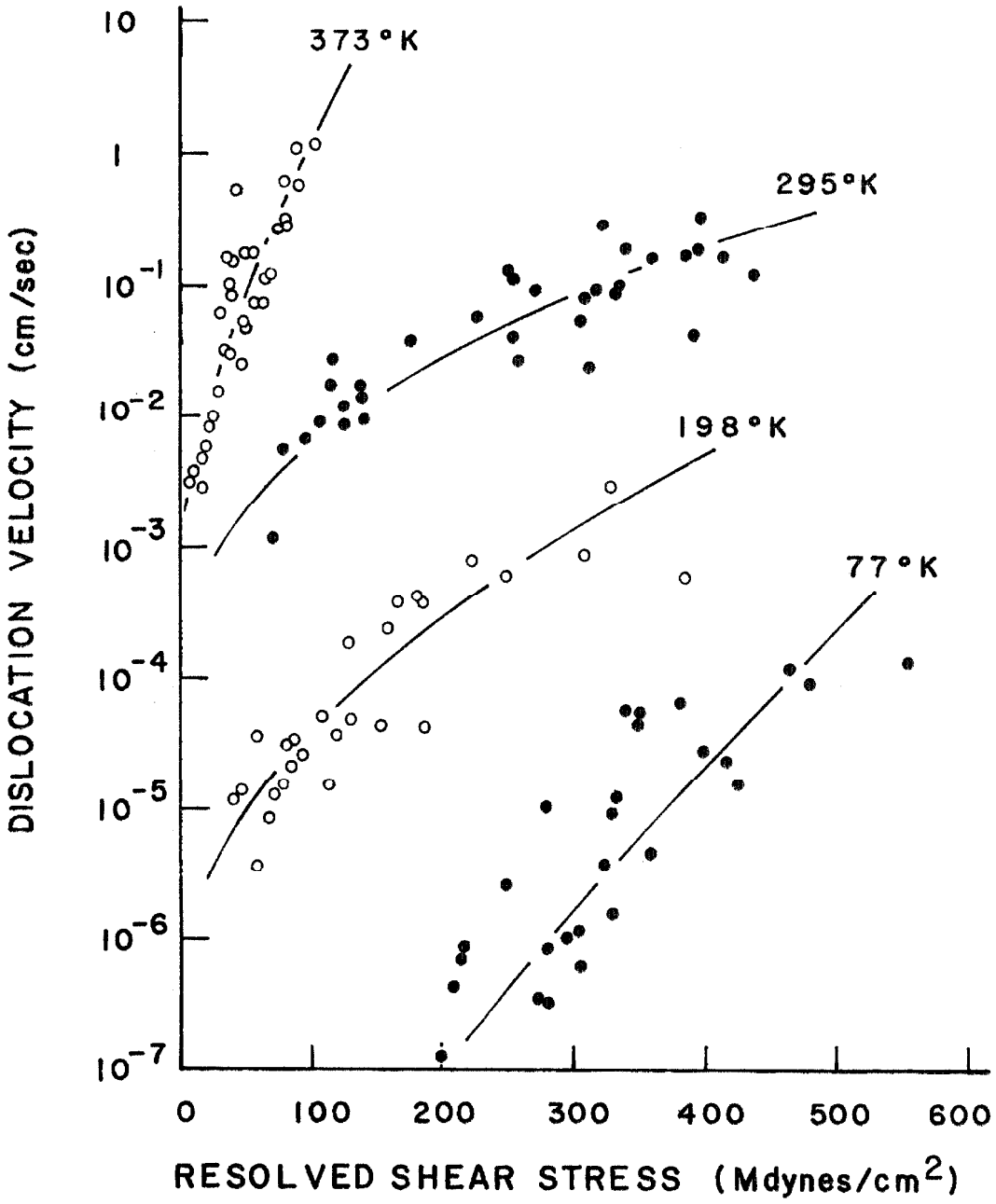

Figure 17. Dislocation Velocity in Iron Single Crystals as Function of Resolved Shear Stress for Several Temperatures.

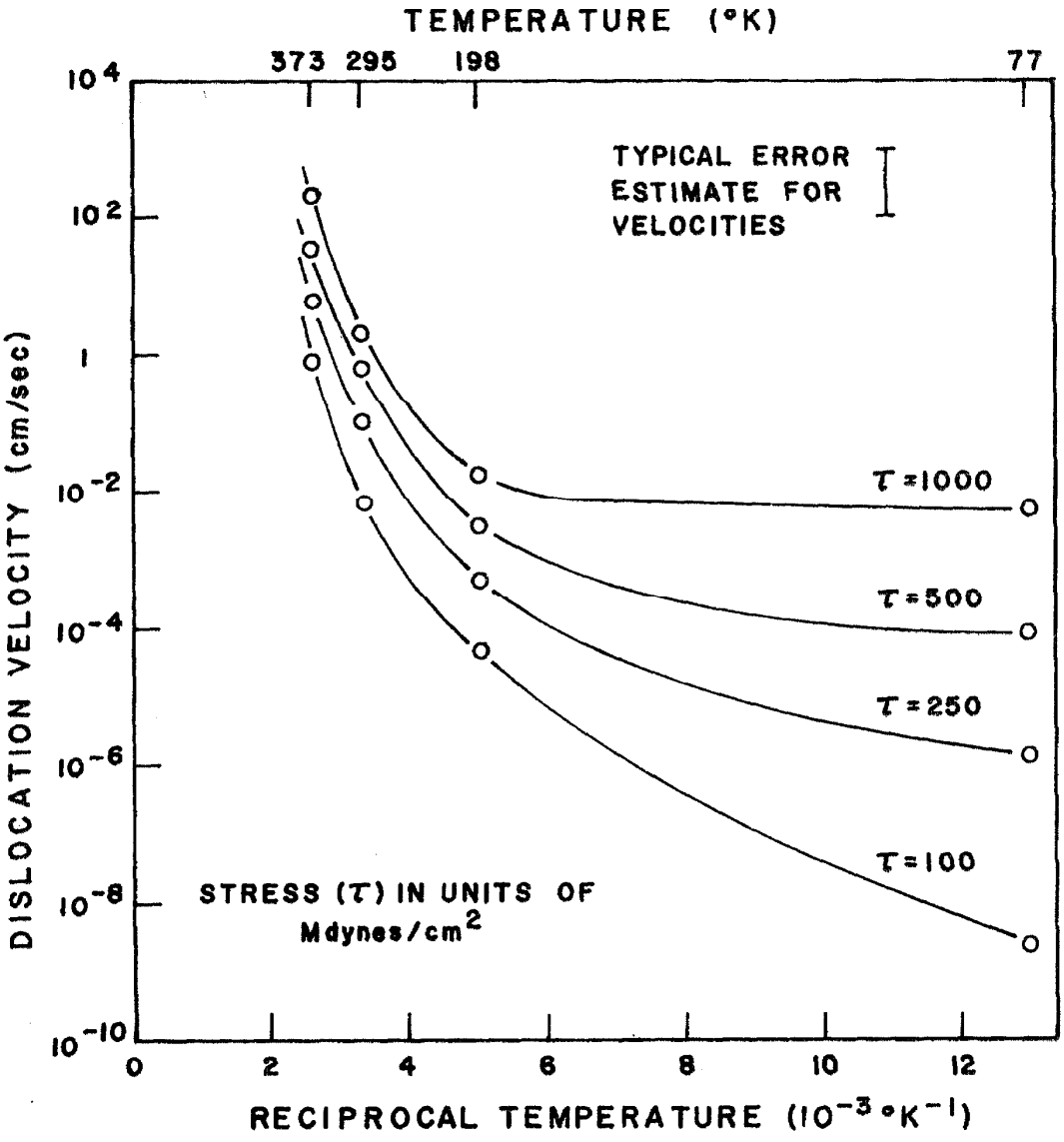

Figure 18. Dislocation Velocity in Iron Single Crystals at Constant Stress as Function of Reciprocal of Temperature.

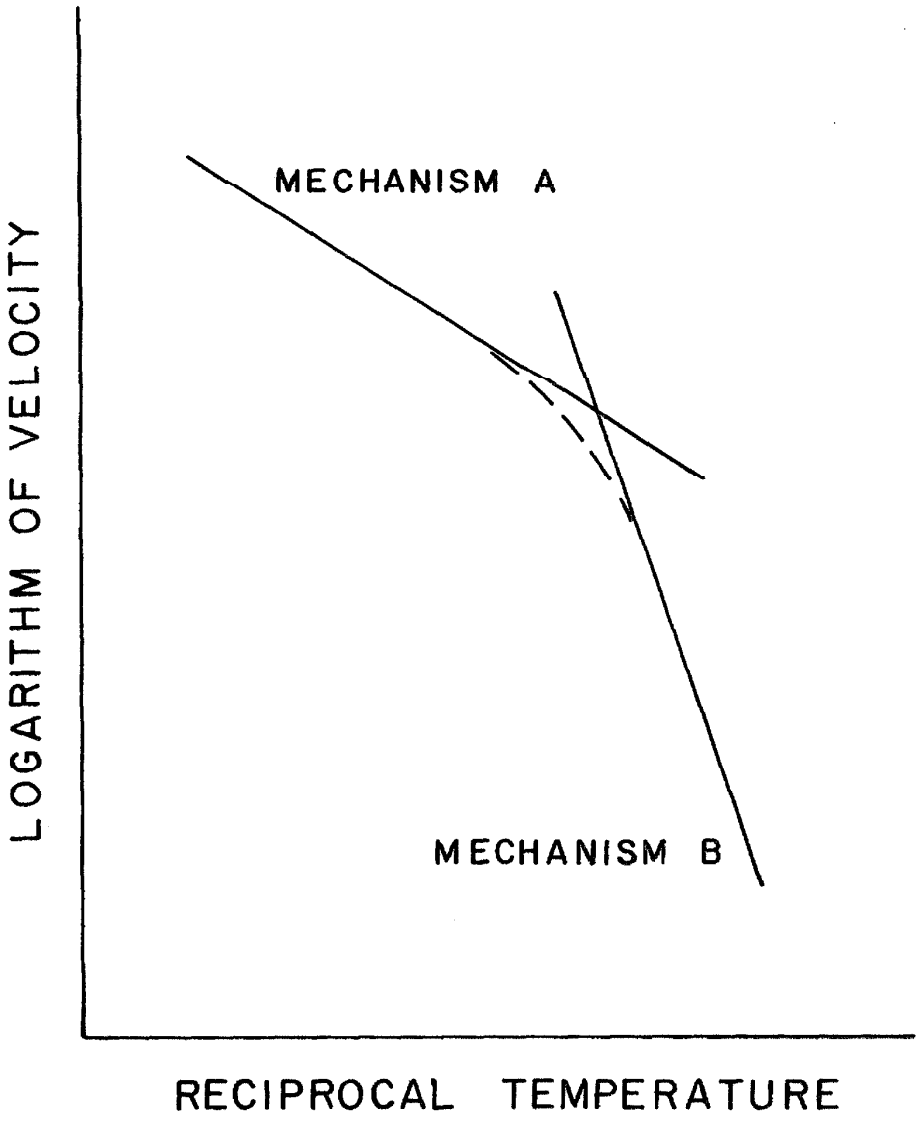

Figure 19. Schematic Diagram of Behavior of Dislocation Velocity when Two Thermal Activation Mechanisms Act Simultaneously.

processes are nearly equal, the true velocity will be somewhat slower than for either process alone. The curvature of the dashed line in Figure 19 is the reverse sense of the curvature of the data curves in Figure 18. There is no way that behavior as represented by the experimental data can be explained by any simple addition of thermally activated processes with temperature independent activation energies.

Another possible reason for the form of the experimental results is the presence of an internal stress (τ_i). If such an internal stress arises from an athermal process, it would have no effect on the form of the curves in Figure 18, but would simply mean that the true values of the stress represented by the curves are slightly different from those given in the figure. Furthermore, the internal stress (τ_i) must be less than the smallest stress for which dislocation displacements were observed. If the internal stress is the same for all temperatures, this would mean that the upper bound for the internal stress is 10 Mdynes/cm^2. If a temperature-dependent internal stress were present in the test specimens, this could account for the deviation from expected behavior shown in Figure 18. However, there is little reason to believe that an internal stress of the required magnitude and with the required temperature dependence would be present in pure iron single crystals. Finally, the deviation from linearity in the curves in Figure 18 increases with increasing stress. One would expect the internal stresses to be least important at large applied stresses.

The remaining possible explanation for the form of the experimental results is a change in v_o with temperature. If the tempera-

ture dependence of v_o is the sole cause of the curvature of the curves in Figure 18, v_o must change by several orders of magnitude between 77^o and 373^oK. This appears to be an unreasonably large change of v_o with temperature.

One must therefore conclude that either the activation energy is very sensitive to the temperature or that the mechanism which controls the dislocation velocity cannot be described by equation [29]. If the activation energy is temperature dependent, it cannot be simply related to the slopes of the curves in Figure 18. The activation energy may be calculated from equation [29] if a value is assumed for v_o. From Table III the extremes of the estimations of v_o are 10^4 and 10^9 cm/sec. Activation energy as a function of temperature was calculated from the data for a uniform stress of 100 Mdynes/cm^2. The resulting curves (Figure 20) represent the limits of the activation energy temperature relationship.

There are no theories which predict an activation energy with a temperature dependence like that shown in Figure 20. The magnitude of the change is much greater than one would expect from Seeger's comments (53) concerning possible increase in activation energy with increasing temperature. Kuhlman-Wilsdorf predicts that the activation energy should decrease with increasing temperature. Inclusion of the entropy contribution to the free energy would also cause the activation energy to be reduced at elevated temperature.

The other point of consideration for comparison between theory and experiment is the stress dependence of the activation energy.

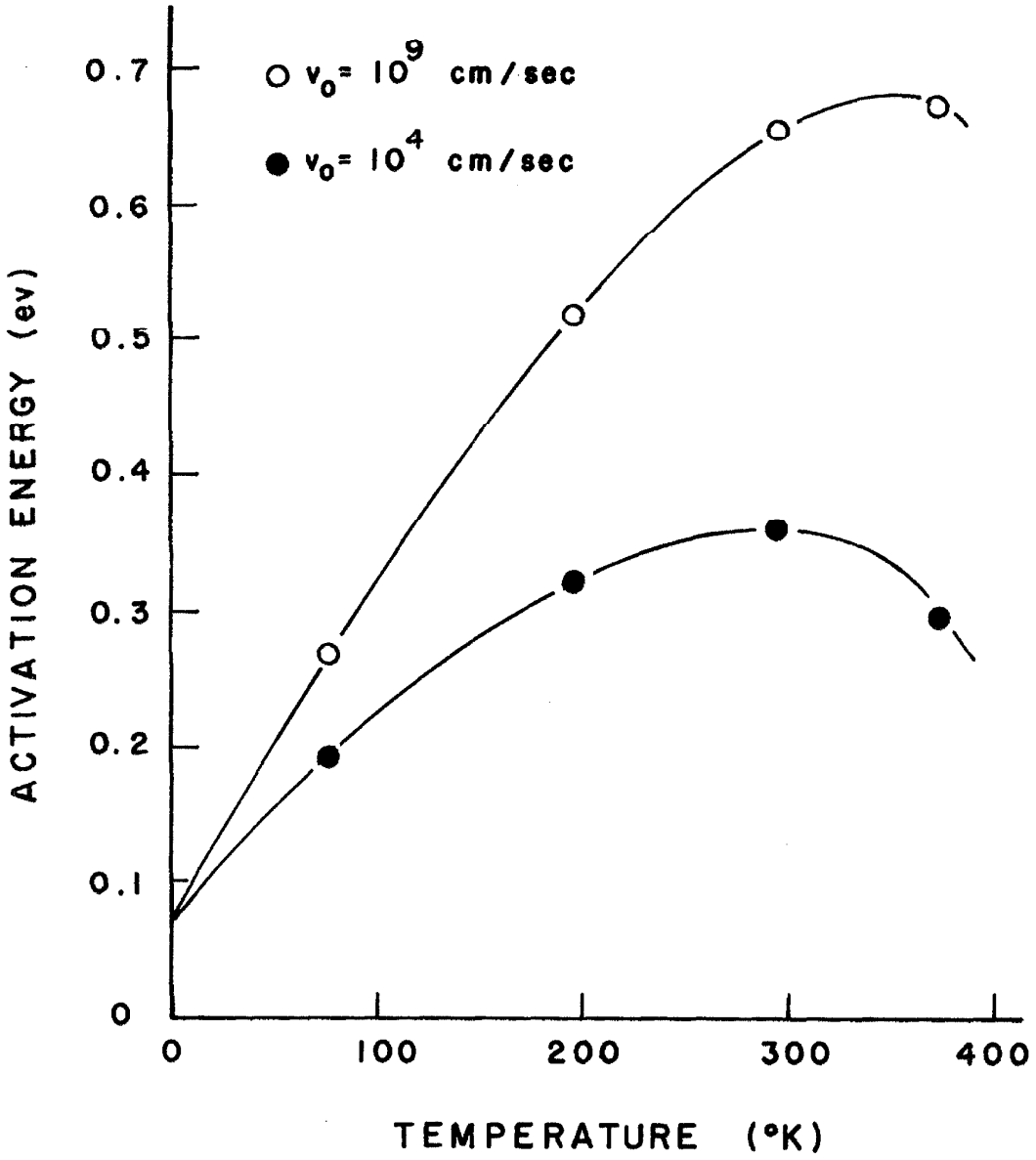

Figure 20. Activation Energy as Function of Temperature for Iron Single Crystals.

The partial derivative of the activation energy with respect to stress at a constant temperature has been defined as the activation volume. Figure 21 presents the curves of activation volume derived from equation [7] using the values of m and τ_o given in Table I. The curves in Figure 21 have the same general form as those in Figure 14 for the Dorn and Rajnak model. The absolute values of the activation volumes derived from the experimental data are in good agreement with most theoretical predictions.

The Fleischer impurity hardening theory predicts the following relationship between stress and temperature for a constant dislocation velocity:

$$(\tau_a/\tau_c)^{\frac{1}{2}} = 1 - \left(\frac{AkT}{F_o b}\right)^{\frac{1}{2}} . \qquad [31]$$

Therefore, a plot of the square root of the stress versus the square root of the temperature for a constant dislocation velocity should be a straight line. The extrapolation of this line to zero temperature gives the quantity τ_c, which is uniquely defined in terms of known parameters. In Figure 22 the square root of the resolved shear stress for a velocity of 10^{-3} cm/sec is plotted against the square root of the temperature. The agreement with a linear relationship is quite good. The value τ_c from Figure 22 is 2300 Mdynes/cm^2. From equations [24 - 27]:

$$\tau_c = \frac{G\Delta\epsilon\,(2c)^{\frac{1}{2}}}{3.86\,(1-\nu)} . \qquad [32]$$

This yields a value for the impurity concentration (c) of 35 ppm by weight. This is considerably greater than the amount of interstitial impurity believed to be present in the specimens. Also, curves cal-

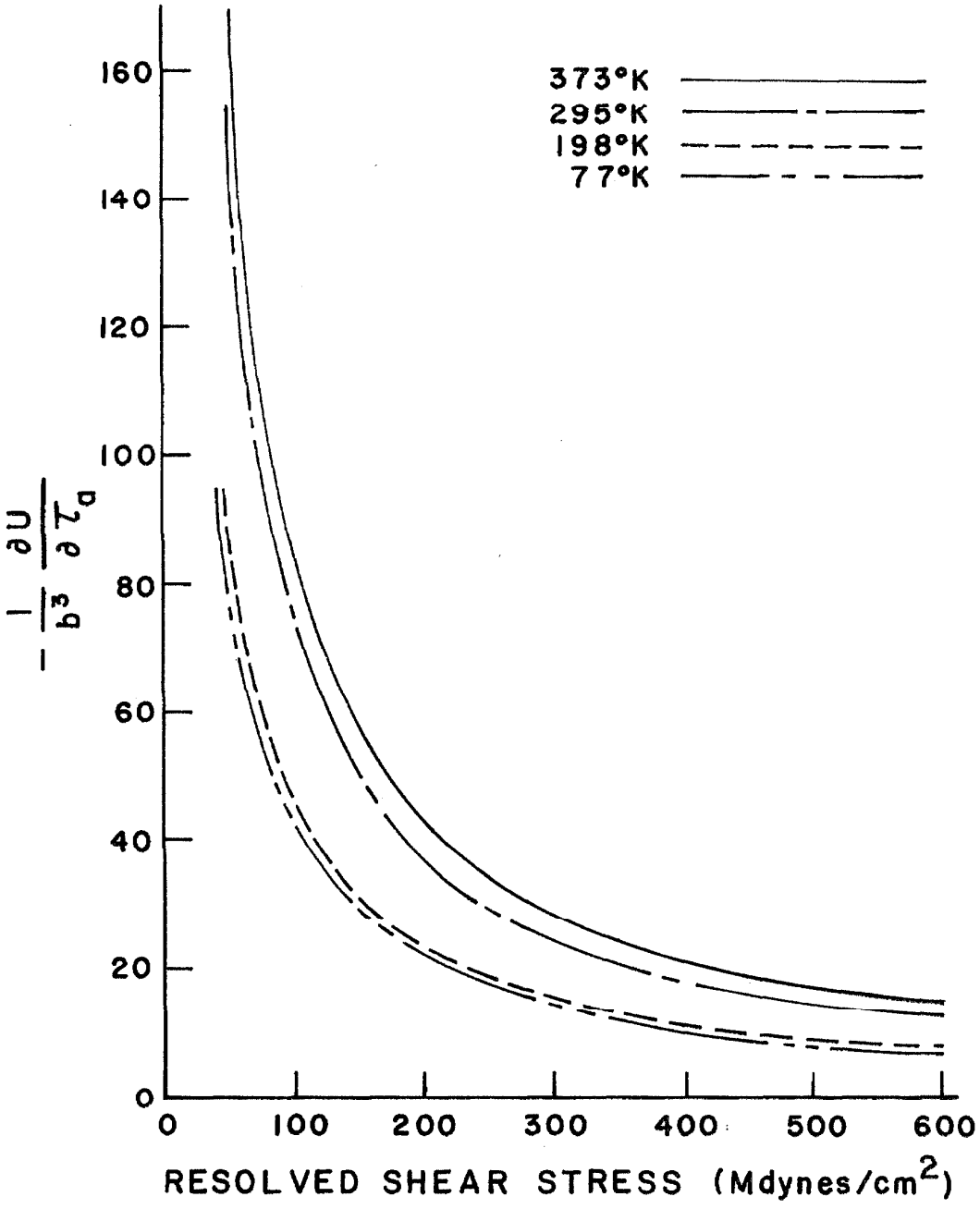

Figure 21. Activation Volume as Function of Applied Stress for Iron Single Crystals.

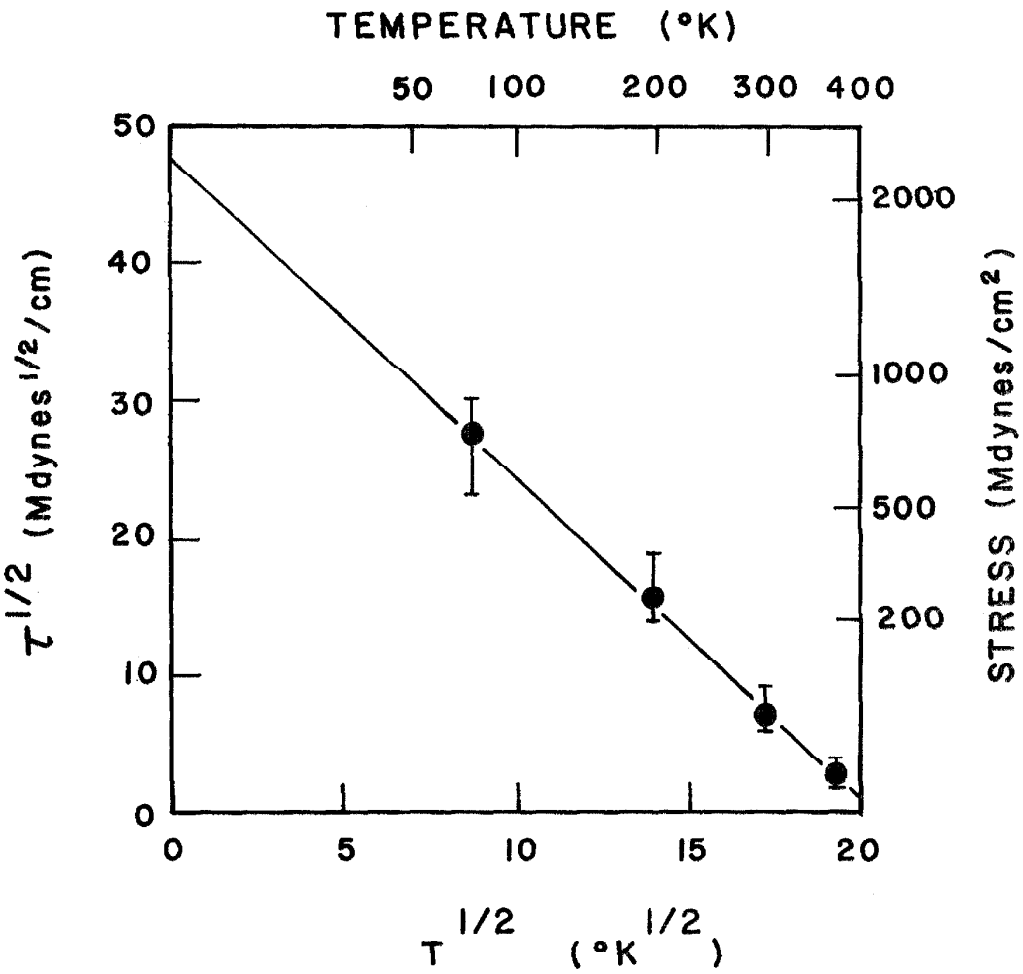

Figure 22. Stress Required to Maintain Dislocation Velocity of 10^{-3} cm/sec as Function of Temperature for Iron Single Crystals.

culated for other velocities using the extrapolation of the experimental measurements do not give the same value of τ_c, and the temperature dependence of the mobility exponent is not the same as predicted by the impurity hardening theory.

Comparison of This Study with Previous Experiments

Several studies, (21, 22, 39, 54) have been made of the mechanical properties of iron single crystals which were essentially identical to the one used in this study. These earlier studies included measurement of the critical resolved shear stress, stress changes for instantaneous changes in the strain rate, and flow stress as a function of temperature. These measurements allow calculation of the apparent stress exponent (m') and the activation volume. Table IV summarizes the results of these measurements.

In cases where direct comparison is possible between the measurements of Stein, et al. and those of Altshuler and Christian, there is considerable disagreement. It is difficult to understand why the two groups of investigators should find such large differences in behavior, because the crystals used in all studies were prepared by Dr. Stein. For each of the critical resolved shear stress values reported in Table IV, a dislocation velocity was calculated from the results of the present study. These values are given in the table. For the critical resolved shear stresses measured by Stein, et al., the velocities at yield are all nearly the same with a mean value of 3.7×10^{-3} cm/sec. Using the equation

$$\dot{\epsilon} = \rho b v \qquad [33]$$

TABLE IV

Results of Other Measurements of Mechanical Properties of Iron Single Crystals

Temperature (°K)	Yield Stress (Mdynes/cm^2)	Velocity at Yield Stress* (cm/sec)	Apparent Stress Exponent
Altshuler and Christian (22)**			
293	180	3.3×10^{-2}	2.75 - 3.4
77	300	4.5×10^{-6}	26
184			40
Stein, Low, and Seybolt (39)			
298	90	7.0×10^{-3}	
198	323	10^{-3}	
77	800	3.0×10^{-3}	
Stein (21)			
298			5
198			10

* The velocities at the yield stress are derived from the results of this study.

** The majority of the study by Altshuler and Christian was upon polycrystalline iron, but they also tested some pure single crystals and found the behavior to be no different.

and $\dot{\epsilon} = 4.5 \times 10^{-5}$ sec^{-1} reported by Stein, the moving dislocation density (ρ) at the yield stress is calculated to be 4.85×10^{5} cm^{-2}. This compares very well with the total dislocation density of 10^{6} cm^{-2} reported by Stein.

The room temperature values of the apparent stress exponents (m') reported in Table IV are reasonably close to the values obtained in this study. However, both groups of investigators found that the apparent exponent increased much faster with decreasing temperature than is indicated by the direct measurement reported here. This disagreement implies that either the assumption that the density of moving dislocations does not change for a sudden change in strain rate is not valid, or that large internal stresses were present in the crystal used to make the strain rate change tests.

The studies listed above also reported values of the activation energy and the activation volume. These quantities were calculated from the measured quantities by making several assumptions about the nature of the deformation process. The assumption is made that the moving dislocation density does not change for abrupt changes in strain rate or for changes in temperature at constant strain. The activation energy and the activation volume as defined in this paper are assumed to be temperature independent. The results reported in this paper indicate that these assumptions are very questionable. Therefore, the activation parameters derived from direct dislocation velocity measurements cannot be meaningfully compared with those derived from indirect tests under the above assumptions.

The parameters derived from this study may also be compared

with those derived by similar experimental methods for other pure BCC materials. Table V shows the results of investigations on molybdenum (35), niobium (55), and tungsten (56). The absolute values of the stress exponents appear to be reasonably consistent with the ones determined for iron. There is a marked tendency for the exponents to decrease as the purity of the material increases, as shown by the results for the zone-refined niobium. With the exception of the results for molybdenum, there appears to be a relatively small change in the exponent near room temperature. This agrees well with the results of this study.

The most interesting point about the results reported for the present study is that the logarithm of the velocity is not a linear function of the reciprocal of the temperature. Since the measurements on molybdenum and tungsten were made at only two temperatures, no determination can be made of how well the behavior of these materials agrees with the functional dependence predicted by the theories. This comparison can be made for the data on niobium. Figure 23 shows the dislocation velocity plotted against reciprocal temperature for a stress of 1000 Mdynes/cm^2 using the data reported by Guberman. These data definitely exhibit the same type of curvature as did the data for iron. Even though long extrapolations of the measured data are required for the construction of Figure 23, the way the stress exponent (m) changes with temperature indicates that what is shown is a real effect. Stein and Low also observed the same type of behavior in Fe-3^o/o Si alloy. It therefore appears that the observed behavior of iron is consistent with the behavior of other BCC materials for which

accurate and complete dislocation mobility measurements have been made.

TABLE V

Dislocation Mobility in B. C. C. Metals

Metal (Reference)	Slip Plane	Temperature (^{o}K)	τ_o (Mdynes/cm^2)	m
Tungsten (Schadler (56))	{110}	298	3080	4.8
	"	77	4250	10.5
Niobium (Guberman (55))	{110}	300	450	15
	"	194	1230	15
	"	77	6450	18
Niobium (zone refined) (Guberman (55))	{110}	300	358	6.7
Molybdenum (Prekel, et al. (35))	{112}	300	562	6.4
	"	77	654	22.3
	{110}	77	888	23.0
Iron (this study)	{110}	373	119	2.56
	"	295	589	2.83
	"	198	4080	2.61
	"	77	2240	6.25

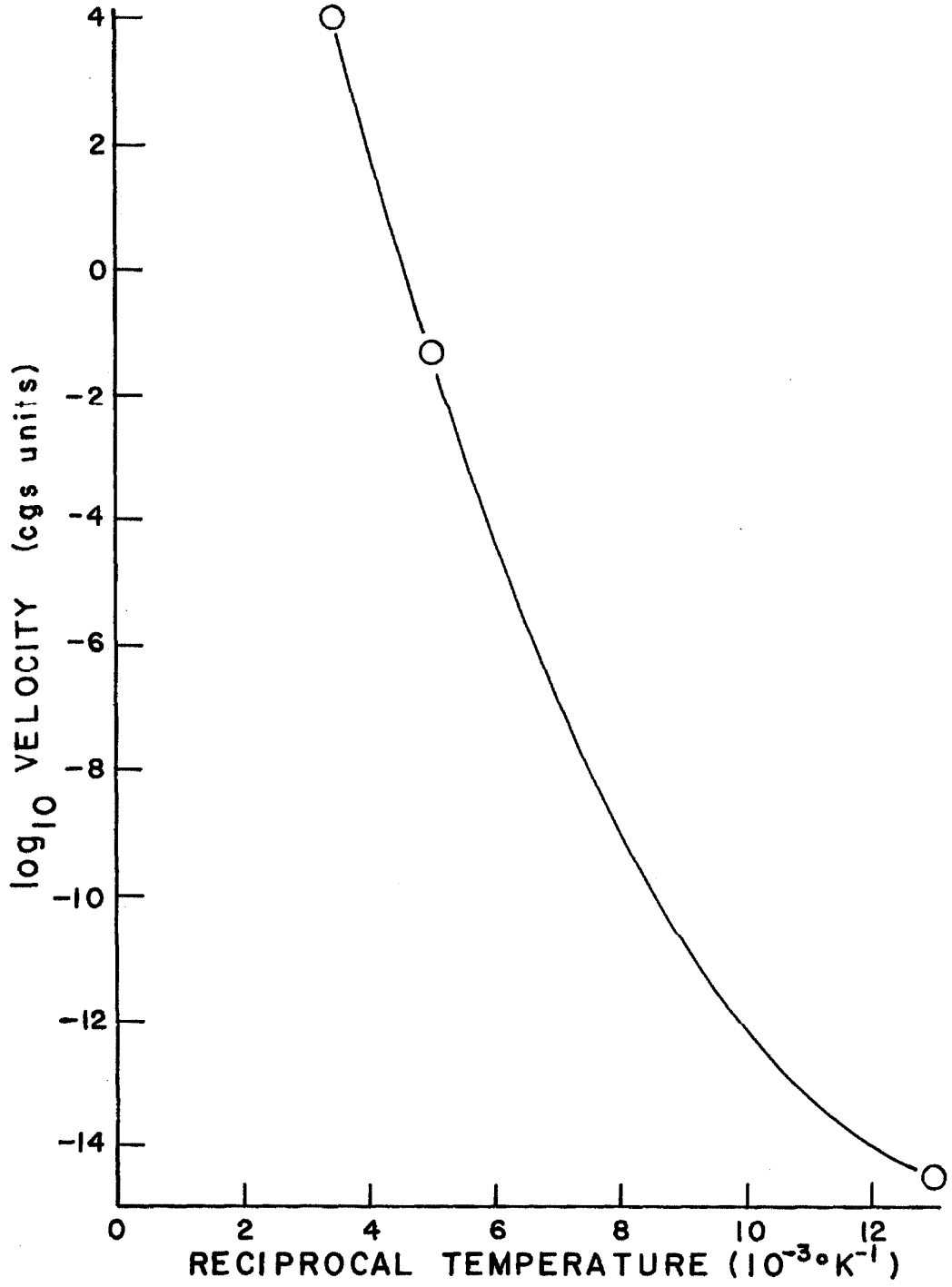

Figure 23. Dislocation Velocity in Niobium Single Crystals for Constant Stress of 1000 Mdynes/cm^2 as Function of Reciprocal of Temperature. Data by Guberman (55).

V. SUMMARY AND CONCLUSIONS

The relationship between dislocation velocity and resolved shear stress was measured for edge dislocations in iron single crystals containing only a few ppm of interstitial impurities. Measurements were made for stresses in the range 10 to 500 Mdynes/cm^2 at temperatures of 393°, 295°, 198°, and 77°K. The velocities were determined by measuring the increase in slip band lengths caused by the application of a short, constant-amplitude load pulse.

The dislocation velocity was found to fit the relationship

$$v = v_o(\tau/\tau_o)^m \qquad [34]$$

for the range of stress covered in this study. The exponent m was found to change from 2.56 at 373°K to 6.25 at 77°K, with nearly all of the change occurring between 198°K and 77°K.

The experimental results were found to be inconsistent with the usual formulations of the thermally activated mechanisms. However, the large changes in dislocation velocity with changing temperature at constant stress indicate that the controlling process is associated with some sort of thermal activation. The results seem to indicate that the activation energy is a function of temperature, but other explanations are probably possible for the observed behavior. The nature of the deviation from predicted behavior in this study is of the same general form as that observed by Stein and Low (6) in Fe-3°/o Si and by Guberman (55) in niobium.

Comparison of the results of this study with indirect measurements on similar crystals indicates that the assumptions made in reducing the data from indirect tests are of questionable validity. Com-

parison of this work with yield stress measurements made by Stein, Low, and Seybolt (39) indicates that the yield stress can correctly be associated with the stress required to maintain a fixed dislocation velocity for a given strain rate. Other yield stress data by Altshuler and Christian (22) are in disagreement with the work of Stein, et al. and also seem to be inconsistent with the work reported here. Values of the exponent obtained from indirect tests are noticeably greater than those found in the present study. The apparent change of the activation energy with temperature and errors in m measured by indirect tests invalidate the assumptions made to determine the activation energy and activation volume from indirect methods.

Suggested Further Work

The most significant possible extension of the current work is to measure the velocities of dislocations in crystals doped with small amounts of carbon in order to directly determine the effect of impurities on the dislocation velocities. The results of this work indicate that a Fleischer type impurity hardening should begin to become important for carbon concentrations as low as 30 ppm by weight.

It would be nice to refine the present data either by reducing the scatter or by increasing the range of the measurements. The former could probably be accomplished by using a crystal oriented close enough to the slip plane to allow observation of the entire dislocation length. If this could be done, uncertainties about the slip plane would be eliminated, and the displacements could be more accurately measured. In addition, the screw dislocation velocities could be measured on a well oriented crystal. Extension of the data

to higher stresses than those used here would require a new testing technique which is not limited by the strength of adhesives. Compression impact is very well suited to this type of test.

The results of this study along with those of Stein and Low in Fe-3^{o}/o Si and Guberman in niobium indicate that current theories of thermal activation have serious shortcomings. Other results, which indicate a breakdown of the critical resolved shear stress law in BCC materials, also indicate a weakness in current theories. Consequently, there is a great need for theoretical explanations for the deformation behavior in BCC materials.

APPENDIX A

Electrolytic Machining

In most electropolishing procedures the spacing between the anode and the cathode is quite large. In these methods, the electropolish flattens the surface either because of the concentrated electric field at surface irregularities or because the electrolysis forms a viscous layer on the surface of the specimen which collects in low spots on the surface and slows the polish. These electropolishing techniques were not suitable for forming the specimens used in this study because they tend to produce spherical surfaces and consequently severely round the edges of the specimens. The electrolytic machining method used in this study places the specimen (anode) very close to the cathode. For sufficiently small anode - cathode spacings, the electric field strength and consequently the cutting rate are inversely proportional to the spacing. This method is capable of forming flat surfaces with only a small amount of rounding at the edges.

The electrolytic machining equipment is shown in Figure 24. The cathode is a stainless steel plate which is spun at the rate of 150-200 RPM. The electrolyte is applied in a stream near the center of the plate. The centrifugal acceleration spreads the electrolyte out into a thin film. The specimen is suspended above the plate on a motor driven slide which feeds the specimen down toward the cathode at a constant rate. The goniometer is used to position the specimen so that the finished surface is correctly oriented.

It is clearly important to keep the spacing between the specimen and the spinning cathode plate small if adequate flattening is going

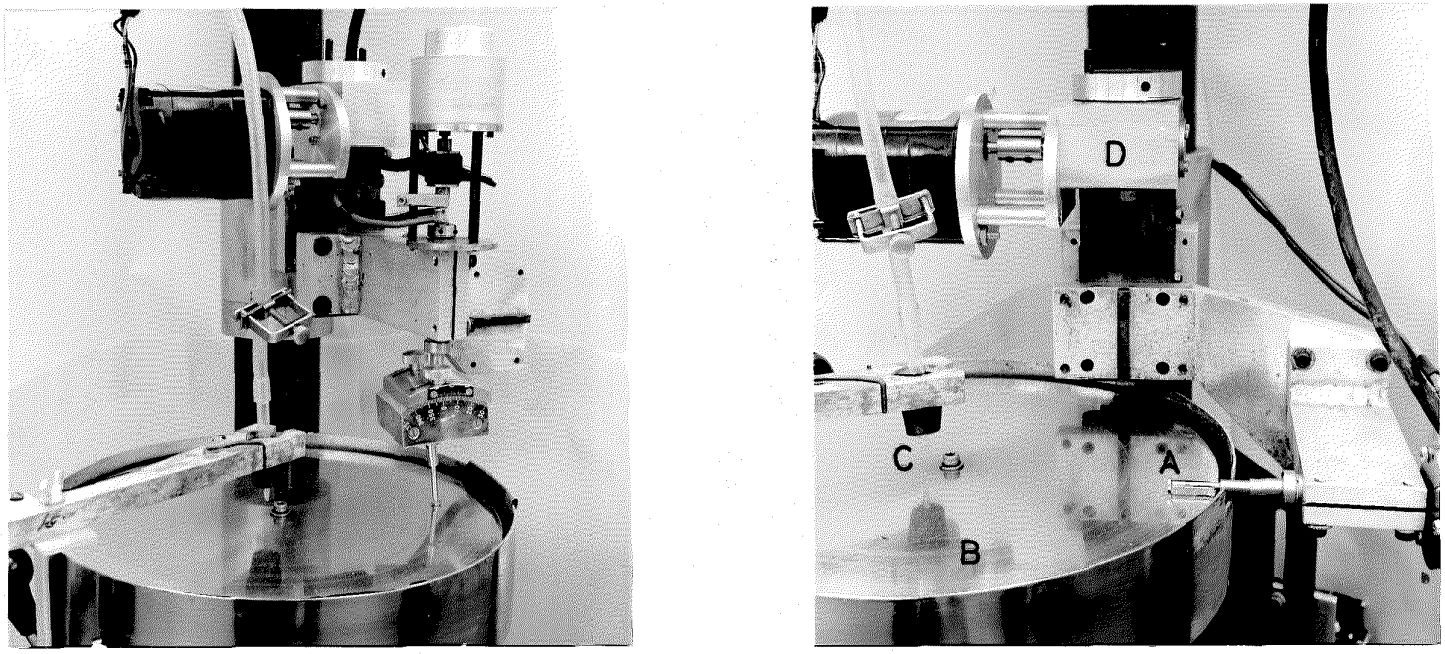

(a) (b)

Figure 24. Electrolytic Machining Apparatus. (a) Arrangement for Facing Operations. (b) Arrangement for Turning Operations. A Specimen, B Cathode Plate, C Nozzle to Supply Electrolyte, D Specimen Feed.

to occur. It is equally obvious that if the spinning plate hits the specimen it can be severely damaged. The runout of the spinning cathode plate on the equipment used is approximately 0.01 mm. This means that the system must be able to flatten sufficiently at a spacing on the order of 0.02 mm or greater. By experimentation it was found that a 1 M solution of ferrous chloride ($FeCl_2$) had the desired properties for the electrolyte. Using this electrolyte, the specimen flattened adequately at spacings between 0.02 and 0.06 mm with a potential of 3 - 3.5 volts across the gap. With the ferrous chloride electrolyte, the cutting rate was a sensitive function of the gap spacing. The cutting rate reached a value of 0.125 mm/min at a spacing of 0.02 mm. The current density at this cutting rate is 6 - 8 amp/cm^2. With the ferrous chloride electrolyte, the material removed from the specimen is plated out onto the cathode in a thin uniform band.

The procedure used in shaping the specimen surface is extremely simple under the conditions described above. The specimen is fed down toward the plate at a constant speed of 0.125 mm/min. The gap spacing decreases and the cutting rate increases until the cutting rate is equal to the feed rate. When this equilibrium is reached, the spacing remains constant and the cutting may be continued until the desired specimen shape and size is achieved. The specimen is rotated about an axis perpendicular to the plate on facing operations. The purpose of this rotation is to smooth out any irregularities in the surface which might be caused by the flow patterns of the electrolyte, and to spread the iron which plates onto the cathode

over a larger area.

The machine was also operated as a lathe. The operation was basically the same as for facing operations, but with the following modifications. The specimen rotation axis was remounted perpendicular to the feed direction. Since the specimen feed had a fixed speed, the feed was operated intermittently on lathing operations because each part of the specimen was cutting for only a fraction of the time. This difficulty could easily be overcome by using a variable speed motor for the specimen feed. The feed speed could then be adjusted to changing situations.

APPENDIX B

Stress State for Anisotropic Torsion Specimens

The matrix of elastic constants for a cubic crystal with orientation given by:

$$X'_1 = [\bar{1}10]\ ;\ X'_2 = [001]\ ;\ X'_3 = [110] \qquad [35]$$

is, for the stiffness moduli:

$$\begin{matrix} C'_{11} & C'_{12} & C'_{13} & 0 & 0 & 0 \\ C'_{12} & C'_{22} & C'_{12} & 0 & 0 & 0 \\ C'_{13} & C'_{12} & C'_{11} & 0 & 0 & 0 \\ 0 & 0 & 0 & C'_{44} & 0 & 0 \\ 0 & 0 & 0 & 0 & C'_{55} & 0 \\ 0 & 0 & 0 & 0 & 0 & C'_{44} \end{matrix} \qquad [36]$$

The C'_{ij}'s defined in terms of the C_{ij}'s where the axes are the cube edges are:

$$\begin{aligned} C'_{11} &= \tfrac{1}{2}(C_{11} + C_{12}) + C_{44} & C'_{12} &= C_{12} \\ C'_{13} &= \tfrac{1}{2}(C_{11} + C_{12}) - C_{44} & C'_{22} &= C_{11} \\ C'_{55} &= \tfrac{1}{2}(C_{11} - C_{12}) & C'_{44} &= C_{44} \end{aligned} \qquad [37]$$

The form of the matrix of compliances is the same as matrix [36].

The S'_{ij}'s defined in terms of the three independent cubic elastic compliances are:

$$\begin{aligned} S'_{11} &= \tfrac{1}{2}(S_{11} + S_{12}) + \tfrac{1}{4} S_{44} & S'_{12} &= S_{12} \\ S'_{13} &= \tfrac{1}{2}(S_{11} + S_{12}) - \tfrac{1}{4} S_{44} & S'_{22} &= S_{11} \\ S'_{55} &= 2(S_{11} - S_{12}) & S'_{44} &= S_{44} \end{aligned} \qquad [38]$$

The problem of finding the exact stress distribution in an anisotropic disc, with axis X_3', subjected to torsion by bonding it between two isotropic rods is not easily solved. However, consideration of two limiting cases indicates that the resolved shear stress on the dislocations is not very much different from what it is for the completely isotropic bar in torsion.

The stress distribution in a circular anisotropic rod in torsion, when no constraints are placed on the displacements of the rod, is exactly the same as for the isotropic circular rod in torsion. This is obvious from the fact that in this situation the entire problem is specified in terms of stresses and resultant forces and moments. Therefore, the same stress distribution is the solution to the problem for any set of elastic constants. The stresses for this problem are then:

$$\tau_{13} = \frac{-2M}{\pi R^4} x_2$$

$$\tau_{23} = \frac{2M}{\pi R^4} x_1 \qquad [39]$$

$$\sigma_1 = \sigma_2 = \sigma_3 = \tau_{12} = 0$$

The strains associated with this stress distribution are:

$$\gamma_{13} = -2(S_{11}-S_{12}) \frac{2M}{\pi R^4} x_2$$

$$\gamma_{23} = S_{44} \frac{2M}{\pi R^4} x_1 \qquad [40]$$

$$\epsilon_1 = \epsilon_2 = \epsilon_3 = \gamma_{12} = 0$$

The displacements derived by integrating the strains and taking all rigid body motions equal to zero are:

$$U_1 = -\frac{(S_{44} + 2(S_{11}-S_{12}))M}{\pi R^4} x_2 x_3$$

$$U_2 = \frac{(S_{44} + 2(S_{11}-S_{12}))M}{\pi R^4} x_1 x_3 \qquad [41]$$

$$U_3 - \frac{(S_{44} - 2(S_{11}-S_{12}))M}{\pi R^4}$$

This means that the anisotropic circular disc warps when subjected to torsion like an elliptic isotropic rod. This solution is clearly not the exact solution to the present problem because the displacement U_3 is incompatible with the displacements of the isotropic rods to which the specimen disc is bonded. However, the true stress in the specimen would approach the stress distribution given by equation [39] as the isotropic rods became very soft compared to the specimen. Since the specimen is bonded with a layer of compliant epoxy resin, the stiffness of the layer adjacent to the specimen is indeed smaller than the stiffness of the specimen.

The opposite limiting case is when the isotropic rods are infinitely rigid and the specimen very thin. In this case we can assume the displacements in the specimen to be:

$$U_1 = -Bx_2x_3$$

$$U_2 = Bx_1x_3 \qquad [42]$$

$$U_3 = 0$$

Differentiating the displacements gives the following strains:

$$\varepsilon_1 = \varepsilon_2 = \varepsilon_3 = \gamma_{13} = 0$$

$$\gamma_{23} = Bx_1 \qquad [43]$$

$$\gamma_{13} = -Bx_2$$

The stresses associated with these strains are:

$$\tau_{23} = C_{44}Bx_1$$

$$\tau_{13} = \tfrac{1}{2}(C_{11}-C_{12})(-Bx_2) \qquad [44]$$

$$\sigma_1 = \sigma_2 = \sigma_3 = \tau_{12} = 0$$

The constant B is evaluated by integrating the stress to find the moment (M):

$$M = \iint C_{44}Bx_1^2 dA - \iint \tfrac{1}{2}(C_{11}-C_{12})(-Bx_2^2)dA \qquad [45]$$

which gives for B in terms of the moment:

$$B = \frac{4M}{R^4\pi(C_{44} + \tfrac{1}{2}(C_{11}-C_{12}))} \quad . \qquad [46]$$

The resolved shear stress acting on dislocations with the $[1\bar{1}1]$ Burgers vector can now be evaluated for the two stress distributions given by equation [39] and equation [44]. Using values for the elastic constants from Mason (57),

$$C_{11} = 2.37\times10^{12} \text{ dynes/cm}^2 \qquad S_{11} = 7.57\times10^{-13} \text{ cm}^2/\text{dyne}$$
$$C_{12} = 1.41\times10^{12} \text{ " } \qquad S_{12} = -2.82\times10^{-13} \text{ " }$$
$$C_{44} = 1.16\times10^{12} \text{ " } \qquad S_{44} = 8.62\times10^{-13} \text{ " } , \qquad [47]$$

the resolved shear stress (τ_r) calculated from equations [39] is:

$$\tau_r = \frac{2Mr}{\pi R^4} \quad , \qquad [48]$$

and calculated from equations [44] is:

$$\tau_r = 0.95\left(\frac{2Mr}{\pi R^4}\right) \quad . \qquad [49]$$

Since the resolved shear stresses for the two cases considered here differ by only 5 percent, the use of the isotropic stresses,

equations [39], does not introduce a very large error into the stress-velocity relations reported in this work. In addition, the measurements were all made at points on the specimen for which the angular relationship relative to the crystal orientation was a constant. This means that although the use of the isotropic stresses introduces a slight error in the absolute magnitude of the stress, the same functional form of the velocity-stress relationship will be observed unless the actual stress distribution differs significantly from being linearly related to the radius.

LIST OF REFERENCES

1. A. H. Cottrell and B. A. Bilby, "Dislocation Theory of Yielding and Strain Ageing in Iron," Proc. Phys. Soc. A 62, 49 (1949).

2. F. C. Fisher, "Application of Cottrell's Theory of Yielding to Delayed Yield in Steel," Trans. ASM 47, 451 (1955).

3. H. Conrad, "On the Mechanism of Yielding and Flow in Iron," J. Iron Steel Inst. 198, 364 (1961).

4. H. Conrad, "Effect of Temperature on Yield and Flow Stress of B. C. C. Metals," Phil. Mag. 5, 745 (1960).

5. H. Conrad and G. Schoeck, "Cottrell Locking and the Flow Stress in Iron," Acta Met. 8, 791 (1960).

6. D. F. Stein and J. R. Low, "Mobility of Edge Dislocations in Silicon-Iron Crystals," J. Appl. Phys. 31, 362 (1960).

7. J. E. Dorn, "Low-temperature Dislocation Mechanisms," Dislocation Dynamics, McGraw-Hill, New York (1968), p. 27.

8. G. Schoeck, "On the Yield Stress in B. C. C. Metals," Acta Met. 9, 382 (1961).

9. J. Helsop and N. J. Petch, "The Stress to Move a Free Dislocation in Alpha Iron," Phil. Mag. 1, 866 (1956).

10. Z. S. Basinski and J. W. Christian, "The Influence of Temperature and Strain Rate of the Flow Stress of Annealed and Decarburized Iron at Subatmospheric Temperatures," Aust. J. Phys. 13, 299 (1960).

11. H. Conrad and S. Frederick, "The Effect of Temperature and Strain Rate on the Flow Stress of Iron," Acta Met. 10, 1013 (1962).

12. B. L. Mordike and P. Haasen, "The Influence of Temperature and Strain Rate on the Flow Stress of α-Iron Single Crystals," Phil. Mag. 7, 459 (1962).

13. R. L. Fleischer, "Rapid Solution Hardening, Dislocation Mobility, and the Flow Stress of Crystals," J. Appl. Phys. 33, 3504 (1962).

14. R. L. Fleischer, "The Flow Stress of Body Centered Cubic Metals: Inherent Lattice Hardening or Solution Hardening?" Acta Met. 15, 1513 (1967).

15. A. Kumar, "Rapid Solution Hardening in B. C. C. Iron and LiF," Acta Met. 16, 333 (1968).

16. A. Seeger, "On the Theory of the Low-Temperature Internal Friction Peak Observed in Metals," Phil. Mag. 1, 651 (1956).

17. A. Seeger and P. Schiller, "Bildung und Diffusion von Kinken als Grundprozess der Versetzungs Bewegung bei der Messung der Inneren Reibung," Acta Met. 10, 348 (1962).

18. A. Seeger and P. Schiller, "Kinks in Dislocation Lines and Their Effects on Internal Friction in Crystals," Physical Acoustics, Academic Press, New York (1966), vol. 3, part A, p. 361.

19. J. Friedel, "On the Elastic Limit of Crystals," Electron Microscopy and Strength of Crystals, Interscience Pub., New York (1963), p. 605.

20. J. E. Dorn and S. Rajnak, "Nucleation of Kink Pairs and the Peierls' Mechanism of Plastic Deformation," Trans. Met. Soc. AIME 230, 1052 (1964).

21. D. F. Stein, "The Effect of Carbon on the Strain-Rate Sensitivity of Iron Single Crystals," Acta Met. 14, 99 (1966).

22. T. L. Altshuler and J. W. Christian, "The Mechanical Properties of Pure Iron Tested in Compression over the Temperature Range 2 to 293 ^{o}K," Phil. Trans. Roy. Soc. A 261, 253 (1967).

23. R. E. Peierls, "Commentary on the 'Peierls-Nabarro Force'," Dislocation Dynamics, McGraw-Hill, New York (1968), p. xiii.

24. R. E. Peierls, "The Size of a Dislocation," Proc. Phys. Soc. A 52, 34 (1940).

25. F. R. N. Nabarro, "Dislocations in a Simple Cubic Lattice," Proc. Phys. Soc. A 59, 256 (1947).

26. F. R. N. Nabarro, "Mechanical Effects of Carbon in Iron," Rep. Conf. on Strength of Solids, Physical Society, London (1948), p. 38.

27. A. Forman and M. Makin, "Dislocation Movement Through Random Arrays of Obstacles," Phil. Mag. 14, 911 (1966).

28. U. F. Kocks, "A Statistical Theory of Flow Stress and Work-hardening," Phil. Mag. 13, 541 (1966).

29. R. J. Arsenault, "Low Temperature Creep of Alpha Iron," Acta Met. 12, 547 (1964).

30. H. D. Guberman and D. N. Beshers, "Amplitude-dependent Internal Friction and Induced Modulus Defect in Purified Iron," Acta Met. 16, 167 (1968).

31. T. Takeuchi and S. Ikeda, "Yield Points and Transient Creeps in Polycrystalline Iron of Very Low Carbon Content," J. Phys. Soc. Japan 18, 488 (1963).

32. T. Takeuchi and S. Ikeda, "Low Temperature Creeps and Delay Times in Iron of Very Low Carbon Content," J. Phys. Soc. Japan 18, 767 (1963).

33. U. E. Wulff, General Electric Report No. 62-LMC-191 (1962).

34. J. C. M. Li, "Kinetics and Dynamics in Dislocation Plasticity," Dislocation Dynamics, McGraw-Hill, New York (1968), p. 87.

35. H. L. Prekel, A. Lawley, and H. Conrad, "Dislocation Velocity Measurements in High Purity Molybdenum," Acta Met. 16, 337 (1968).

36. H. Conrad, "Comment on 'The Effect of Carbon on the Strain Rate Sensitivity of Iron Single Crystals'," Acta Met. 15, 147 (1967).

37. D. F. Stein, "Reply to Comment on 'The Effect of Carbon on the Strain Rate Sensitivity of Iron Single Crystals'," Acta Met. 15, 150 (1967).

38. C. G. Dunn and G. C. Nonken, "Production of Oriented Single-Crystal Silicon Iron Sheet," Metal Progress 64, 71 (1953).

39. D. F. Stein, J. R. Low, and A. U. Seybolt, "The Mechanical Properties of Iron Single Crystals Containing Less than 5×10^{-3} ppm Carbon," Acta Met. 11, 1253 (1963).

40. C. L. Formby, "The Effect of Impurities upon Cross-slip in Iron," Phil. Mag. 14, 745 (1966).

41. T. L. Russell, D. S. Wood, and D. S. Clark, First Interim Technical Report under Office of Ordnance Research, Contract No. DA-04-495-ORD-171, California Institute of Technology (1955).

42. D. P. Pope, T. Vreeland, Jr., and D. S. Wood, "Mobility of Edge Dislocations in the Basal-Slip System of Zinc," J. Appl. Phys. 38, 4011 (1967).

43. J. A. Gorman, "The Mobility of Dislocations in High Purity Aluminum," Ph. D. Thesis, California Institute of Technology, Pasadena, California (1968).

44. J. M. Schultz and R. W. Armstrong, "Seeing Dislocations in Zinc," Phil. Mag. 10, 497 (1964).

45. J. B. Newkirk, "The Observation of Dislocations and Other Imperfections by X-Ray Extinction Contrast," Trans. Met. Soc. AIME 215, 483 (1959).

46. A. P. L. Turner, T. Vreeland, Jr., and D. P. Pope, "Experimental Techniques for Observing Dislocations by the Berg-Barrett Method," Acta Cryst. A24, 452 (1968).

47. D. P. Pope, T. Vreeland, Jr., and D. S. Wood, "Comparison System for Microscope Images," Rev. Sci. Instr. 37, 377 (1966).

48. A. R. Rosenfield and G. T. Hahn, "Linear Arrays of Moving Dislocations Emitted by a Source," Dislocation Dynamics, McGraw-Hill, New York (1968), p. 255.

49. H. Suzuki, "Motion of Dislocations in Body-Centered Cubic Crystals," Dislocation Dynamics, McGraw-Hill, New York (1968), p. 679.

50. P. Guyot and J. E. Dorn, "A Critical Review of the Peierls Mechanism," Cana. J. Phys. 45, 983 (1967).

51. T. Jøssang, K. Skylstad, and J. Lothe, "Theory of Thermal Activation of Dislocations over the Peierls Barrier in a Revised Seeger-Donth Formulation," The Relation Between the Structure and Mechanical Properties of Metals, Her Majesty's Stationery Office, London (1963), p. 527.

52. D. Kuhlman-Wilsdorf, "Frictional Stress Acting on a Moving Dislocation an an Otherwise Perfect Crystal," Phys. Rev. 120, 773 (1960).

53. A. Seeger, "Discussion of Paper Presented by H. Suzuki," Dislocation Dynamics, McGraw-Hill, New York (1968), p. 694.

54. D. F. Stein and J. R. Low, "Effects of Orientation and Carbon on the Mechanical Properties of Iron Single Crystals," Acta Met. 14, 1183 (1966).

55. H. D. Guberman, "Stress Dependence of Dislocation Velocity in Single Crystal Niobium," Acta Met. 16, 713 (1968).

56. H. W. Schadler, "Mobility of Edge Dislocations on {110} Planes in Tungsten Single Crystals," Acta Met. 12, 861 (1964).

57. W. P. Mason, Physical Acoustics and the Properties of Solids, Van Nostrand, Princeton, N. J. (1958), p. 358.